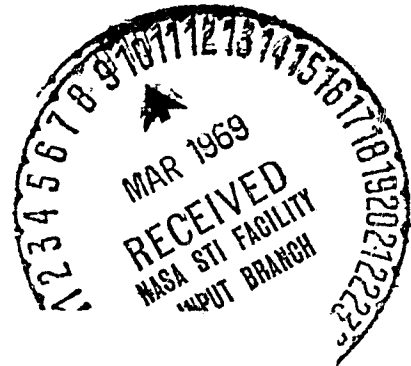


General Disclaimer

One or more of the Following Statements may affect this Document

- This document has been reproduced from the best copy furnished by the organizational source. It is being released in the interest of making available as much information as possible.
- This document may contain data, which exceeds the sheet parameters. It was furnished in this condition by the organizational source and is the best copy available.
- This document may contain tone-on-tone or color graphs, charts and/or pictures, which have been reproduced in black and white.
- This document is paginated as submitted by the original source.
- Portions of this document are not fully legible due to the historical nature of some of the material. However, it is the best reproduction available from the original submission.



ELECTRO-OPTICAL SYSTEMS, INC.
A XEROX COMPANY
PASADENA, CALIFORNIA 91107 • 213/351-2351

N 69-19075

FACILITY FORM 602

(ACCESSION NUMBER)	65	(THRU)	1
(PAGES)	CA-100209	(CODE)	09
(NASA CR OR TMX OR AD NUMBER)		(CATEGORY)	

95221728293037

Third Quarterly Progress Report

THERMIONIC RESEARCH AND DEVELOPMENT PROGRAM

Prepared for
Jet Propulsion Laboratory
California Institute of Technology
4800 Oak Grove Drive
Pasadena, California
Attention: Mr. Lou Jacques

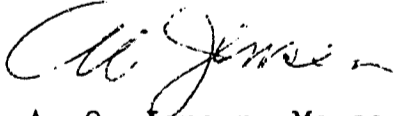
Contract 952217

EOS Report 4006-Q-3

3 February 1969

Prepared by
D. L. Jacobson
R. W. Hamerdinger

Approved by



A. O. Jensen, Manager
Advanced Technologies Division



ELECTRO - OPTICAL SYSTEMS, INC.

A XEROX COMPANY

This work was performed for the Jet Propulsion Laboratory,
California Institute of Technology, sponsored by the
National Aeronautics and Space Administration under
Contract NAS7-100.

CONTENTS

1.	INTRODUCTION	1
2.	ELECTRODE MATERIALS INVESTIGATION (TASK I)	2
2.1	Rhenium	2
2.2	Tungsten Alloy Electrode Materials	9
3.	ELECTRODE MATERIALS INVESTIGATION (TASK II)	29
3.1	Vacuum Emission Vehicle	29
3.2	Thermionic Devices	36
4.	LOW-TEMPERATURE (1700° - 1800° K) CYLINDRICAL CONVERTER (TASK III)	40
4.1	Fabrication and Assembly Procedure of the Cylindrical Converters	42
4.2	Instrumentation and Cylindrical Converter Test Procedures	45
4.3	Performance Testing of SN109CA	49
4.4	Performance Testing of SN109CB	49
4.5	Correlation and Comparison of Cylindrical Converters SN109CA and SN109CB to Planar Converter SN109	54
	REFERENCES	60

ILLUSTRATIONS

1	Rhenium Boule Face Sketch (4:1) Showing Seven Grains of Various Orientation	3
2	Laue Back-Reflection X-Ray Film Print of Grain #1	7
3	Laue Back-Reflection X-Ray Film Print of Grain #6	8
4	Schottky Plots of 95% W/5% Re From Vacuum Emission Vehicle Measurements (Previously High-Fired at 2373°K for 1 Hour)	10
5	Schottky Plot of 85% W/15% Re From Vacuum Emission Vehicle Measurements (Previously High-Fired at 2375°K for 1 Hour)	11
6	Schottky Plot of 95% W/5% Ta From Vacuum Emission Vehicle Measurements (Previously High-Fired at 2323°K for 1/2 Hour)	12
7	Schottky Plot of 90% W/10% Ta From Vacuum Emission Vehicle Measurements (Previously High-Fired at 2333°K for 1 Hour)	13
8	Schottky Plot of 74% W/26% Ta From Vacuum Emission Vehicle Measurements (Previously High-Fired at 2333°K for 1 Hour)	14
9	Schottky Plots of 99% W/1% Ir From Vacuum Emission Vehicle Measurements (Previously High-Fired at 2123°K for 2.5 Hours)	15
10	Schottky Plots of 95% W/2% Ir From Vacuum Emission Vehicle Measurements (Previously High-Fired at 2323°K for 1/2 Hour)	16
11	Thermionic Emission Microscope Mosaic of Pure Tungsten (Magnification 42.5X; $T_E = 2003^\circ\text{K}$)	19
12	Thermionic Emission Microscope Mosaic of 95% W/5% Re (Magnification 42.5X; $T_E = 1953^\circ\text{K}$)	20
13	Thermionic Emission Microscope Mosaic of 85% W/15% Re (Magnification 42.5X; $T_E = 2063^\circ\text{K}$)	21
14	Thermionic Emission Microscope Mosaic of 95% W/5% Ta (Magnification 42.5X; $T_E = 2003^\circ\text{K}$)	22
15	Thermionic Emission Microscope Mosaic of 90% W/10% Ta (Magnification 42.5X; $T_E = 2053^\circ\text{K}$)	23

ILLUSTRATIONS (contd)

16	Thermionic Emission Microscope Mosaic of 74% W/26% Ta (Magnification 42.5X; $T_E = 2003^\circ\text{K}$)	24
17	Thermionic Emission Microscope Mosaic of 99% W/1% Ir (Magnification 42.5X; $T_E = 2105^\circ\text{K}$)	25
18	Thermionic Emission Microscope Mosaic of 98% W/2% Ir (Magnification 42.5X; $T_E = 2003^\circ\text{K}$)	26
19	Thermionic Emission Microscope Mosaic of 97.5% W/2.5% Os (Magnification 42.5X; $T_E = 2053^\circ\text{K}$)	27
20	Thermionic Emission Microscope Mosaic of 95% W/5% Os (Magnification 42.5X; $T_E = 2076^\circ\text{K}$)	28
21	Schottky Plot of 75% Tungsten/25% Rhenium Sample I From Vacuum Emission Vehicle Measurements	30
22	Schottky Plot of 75% Tungsten/25% Rhenium Sample II From Vacuum Emission Vehicle Measurements	31
23	Schottky Plot of 75% Tungsten/25% Rhenium Sample III From Vacuum Emission Vehicle Measurements	32
24	Schottky Plots of CVD 75% W/25% Re Sample IV From Vacuum Emission Vehicle Measurements	33
25	Schottky Plot of CVD 75% W/25% Re Sample V From Vacuum Emission Vehicle Measurements	34
26	Schottky Plots of CVD 75% W/25% Sample VI From Vacuum Emission Vehicle Measurements	35
27	Potential Application of EOS Cylindrical Converter (Multiconverter Array)	41
28	Cylindrical Converter Subassemblies	43
29	Completed SN109CA Diode Assembly	46
30	Electrical Circuit For DC Performance Testing of Thermionic Cylindrical Converters	47
31	Performance Plot of SN109CA Cylindrical Converter Taken at the Design Emitter Temperature of 1800°K (true hohlraum)	50
32	Current Optimization Plot of SN109CA Taken at the Design Operating Emitter Temperature of 1800°K (true hohlraum)	51
33	Performance Plot of SN109CA Cylindrical Converter Taken at an Emitter Temperature of 1700°K (true hohlraum)	52
34	Current Optimization Plot of SN109CA Taken at an Emitter Temperature of 1700°K (true hohlraum)	53

ILLUSTRATIONS (contd)

35	Performance Plots of SN109CB Taken at the Design Emitter Temperature of 1800°K (true hohlraum)	55
36	Current Optimization Plot of SN109CB Taken at the Design Operating Emitter Temperature of 1800°K (true hohlraum) and a Constant Voltage Output of 0.4 Volt	56
37	Performance Plot of SN109CB Taken at 1700°K (true hohlraum)	57
38	Current Optimization Plot of SN109CB Taken at an Emitter Temperature of 1700°K (true hohlraum) and a Constant Voltage Output of 0.3 Volt	58

SECTION 1

INTRODUCTION

The work reported in this, the third quarterly progress report, is being performed under JPL Contract 952217, a 12-month, three-task program of advanced thermionic converter development.

The first task consists of an investigation of single-crystal rhenium and tungsten alloy materials of the following composition: 85% W/15% Re, 95% W/5% Re, 95% W/5% Os, 97.5% W/2.5% Os, 99% W/1% Ir, 98% W/2% Ir, 95% W/5% Ta, 90% W/10% Ta, and 74% W/26% Ta. The purpose of the investigation is to yield a high bare work function surface. Specific investigations include vacuum emission vehicle determination of the effective work functions and examination of electrode surfaces using a thermionic emission microscope. Metallographic examinations are also included.

Task II consists of the investigation of CVD W/22-26 Re electrodes. Bare work function measurements are made with the vacuum emission vehicle, and the electrode surface is examined with the thermionic emission microscope. The electrode material is then incorporated into a variable parameter vehicle, a planar converter, and a cylindrical converter.

Task III completes the program effort with the design, fabrication, and testing of CVD rhenium-electrode cylindrical thermionic converters for the principal purpose of providing a performance comparison between planar and cylindrical geometries.

SECTION 2

ELECTRODE MATERIALS INVESTIGATION (TASK I)

2.1 RHENIUM

In EOS Report 4006-Q-1, it was reported that Linde Crystal Products Division of Union Carbide had attempted to grow a boule of single-crystal rhenium with the (0001) crystallographic plane oriented parallel to the end face of the boule. The resulting boule exhibited several grains, as shown in Fig. 1, which is an approximate reproduction of a sketch supplied by Linde. The crystallographic orientation of each grain was determined by Linde and the results were presented to EOS as reproduced in Table I. Since the (0001) crystallographic orientation was of prime importance for evaluation, it was necessary to cut discs from the boule which would expose at least one grain exhibiting the (0001) orientation. The boule provided two samples which were examined in the thermionic emission microscope to determine the effective work function of each grain. The work function of grain No. 1 was found to be 5.26 eV at 2053°K. Wichner and Pigford (Ref. 1) reported a Richardson work function of 5.59 eV, over the temperature range 1688° to 2294°K, which, when converted to effective work function, is 5.52 eV for (0001) rhenium. Because of this inconsistency, the samples were reexamined by Laue back-reflection X-ray techniques by two independent sources to determine the crystallographic orientation of each grain. The results were then compared with that provided by Linde (Table I). The three analyses are tabulated in Table II. Since the boule was tilted by six and four degrees when sliced, the information in Table I will be slightly different from the nominal values of Table II. The results of the two independent analyses showed that grain No. 1 was not of the (0001) crystallographic orientation as claimed by Linde Crystal Products, but rather of the (10 $\bar{1}$ 0) orientation. Grain No. 2 was not examined by Vendor I, and grains 2 and 3 were not examined by Vendor II.

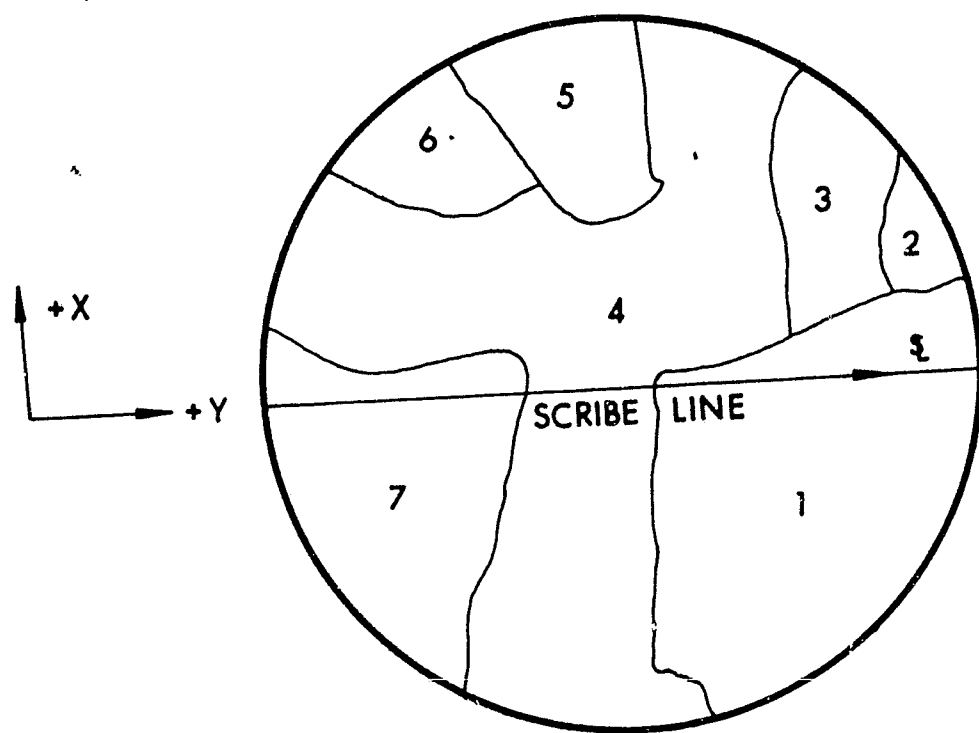


Figure 1. Rhenium Boule Face Sketch (4:1) Showing Seven Grains of Various Orientation

TABLE I
 RESULTS OF LAUE BACK-REFLECTION DETERMINATIONS OF THE ORIENTATION OF
 CRYSTAL PLANE NORMALS WITH RESPECT TO THE BOULE FACE NORMAL AND SCRIBE LINE


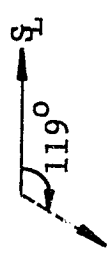
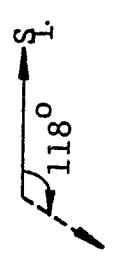
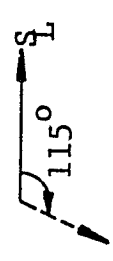
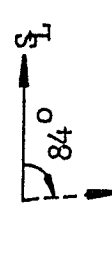


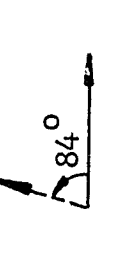
Area	Plane Normal	Degree Tilt (y)	Degree Tilt (x)	Direction of a Second Plane Normal	
1	(0001)	+6°	-4°		(10 $\bar{1}$ 1)
2	(10 $\bar{1}$ 1)	+11-1/2°	+8-1/2°		(0001)
3	(0001)	-1°	+3°		(10 $\bar{1}$ 1)
4	(0001)	+2°	+19-1/2°		(10 $\bar{1}$ 1)
5	(0001)	-6-1/2°	+12°		(10 $\bar{1}$ 1)
6	(0001)	-17°	+11°		(10 $\bar{1}$ 1)
7	(10 $\bar{1}$ 1)	+12°	+29°		(0001)

TABLE II

RESULTS OF LAUE BACK-REFLECTION DETERMINATIONS OF THE ORIENTATION OF THE CRYSTAL PLANE NORMAL WITH RESPECT TO THE SAMPLE FACE NORMAL

Grain	Linde Crystal Products		Source I		Source II	
	Pole Type	Angle of Pole From Face Normal	Pole Type	Angle of Pole From Face Normal	Pole Type	Angle of Pole From Face Normal
1	(0001)	0°	(10 $\bar{1}$ 0)	0°	(10 $\bar{1}$ 0)	1°
2	(10 $\bar{1}$ 0)	~13°	-	-	-	-
3	(0001)	~10°	(0001)	10°	-	-
4	(0001)	~23°	(0001)	22°	(0001)	23°
5	(0001)	~20°	(0001)	18°	(0001)	18°
6	(0001)	~27°	(0001)	27°	(00 $\bar{1}$ 1)	27°
7	(10 $\bar{1}$ 1)	~34°	(10 $\bar{1}$ 0)	45°	(10 $\bar{1}$ 0)	16°

Disagreement is also seen among the results for grain No. 7. Wichner and Pigford (Ref. 1) reported a Richardson work function of 5.15 eV for $(10\bar{1}0)$ rhenium over the temperature range 1688° to 2294°K , which, when converted into an effective value, is 5.22 eV. This compares within experimental error (± 0.04 eV) to the effective work function value of 5.26 eV at 2053°K determined from thermionic emission microscope/Faraday cage measurements.

Figures 2 and 3 are film prints of Laue back-reflection X-ray patterns. Figure 2 was generated from grain No. 1 showing the rectangular symmetry of the $(10\bar{1}0)$ crystallographic orientation. This can be contrasted with the obvious sixfold symmetry of the (0001) orientation of grain No. 6 shown in Fig. 3. Figure 3 was produced with the sample rotated by 27° so that the complete diffraction pattern was visible.

The averaged effective work functions of the major grains as determined from the thermionic emission microscope/Faraday cage measurements are shown in Table III along with the crystallographic orientations.

TABLE III
EFFECTIVE WORK FUNCTIONS FOR RHENIUM AT 2053°K FROM
THERMIONIC EMISSION MICROSCOPE MEASUREMENTS AND
CRYSTALLOGRAPHIC ORIENTATION

<u>Grain No.</u>	<u>ϕ_{eff}(eV)</u>	<u>Pole Type</u>	<u>Angle of Pole from Surface Normal</u>
1	5.26	$(10\bar{1}0)$	$< 1^{\circ}$
4	4.92	(0001)	23°
5	5.06	(0001)	18°
6	5.07	(0001)	27°

005399

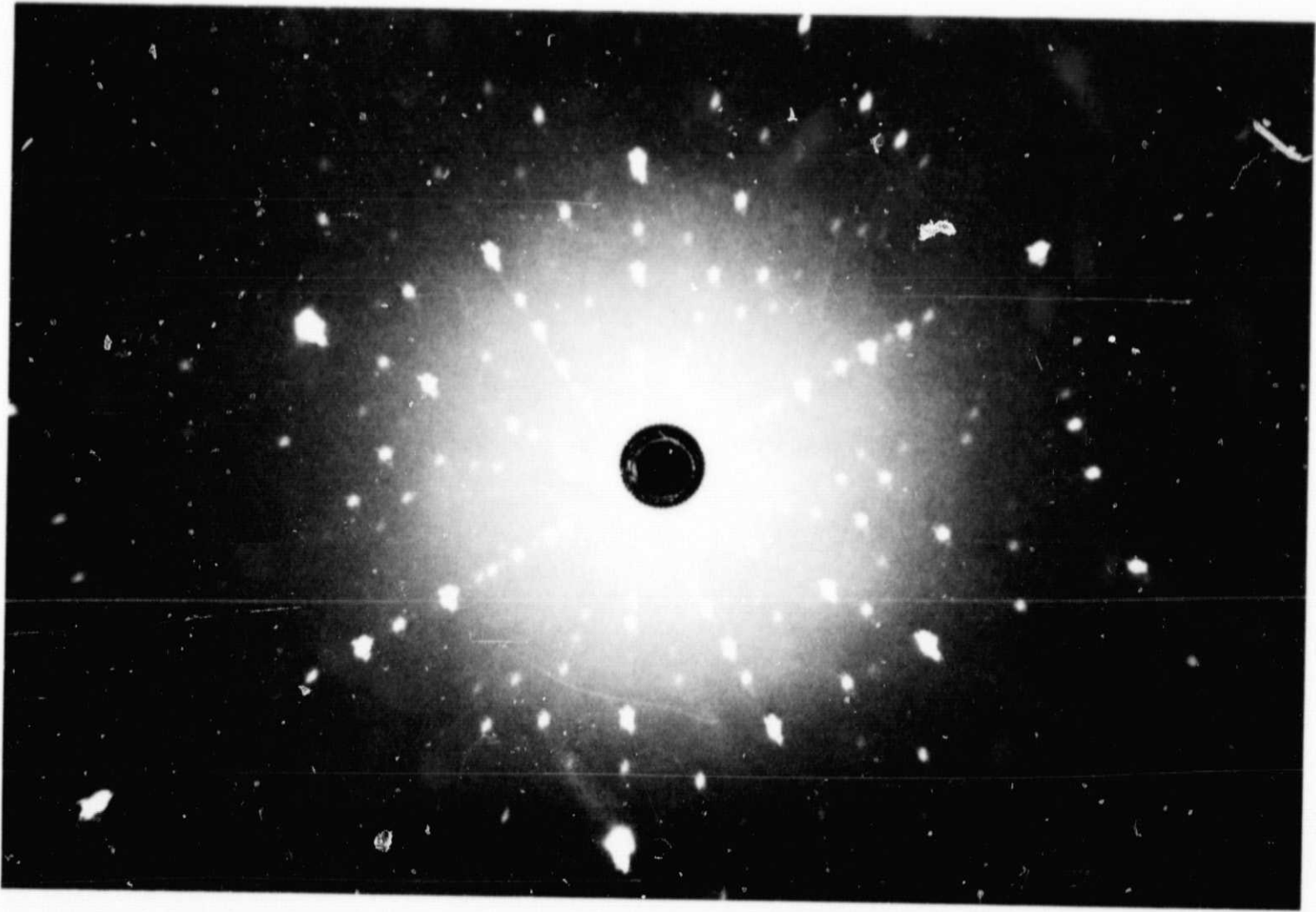
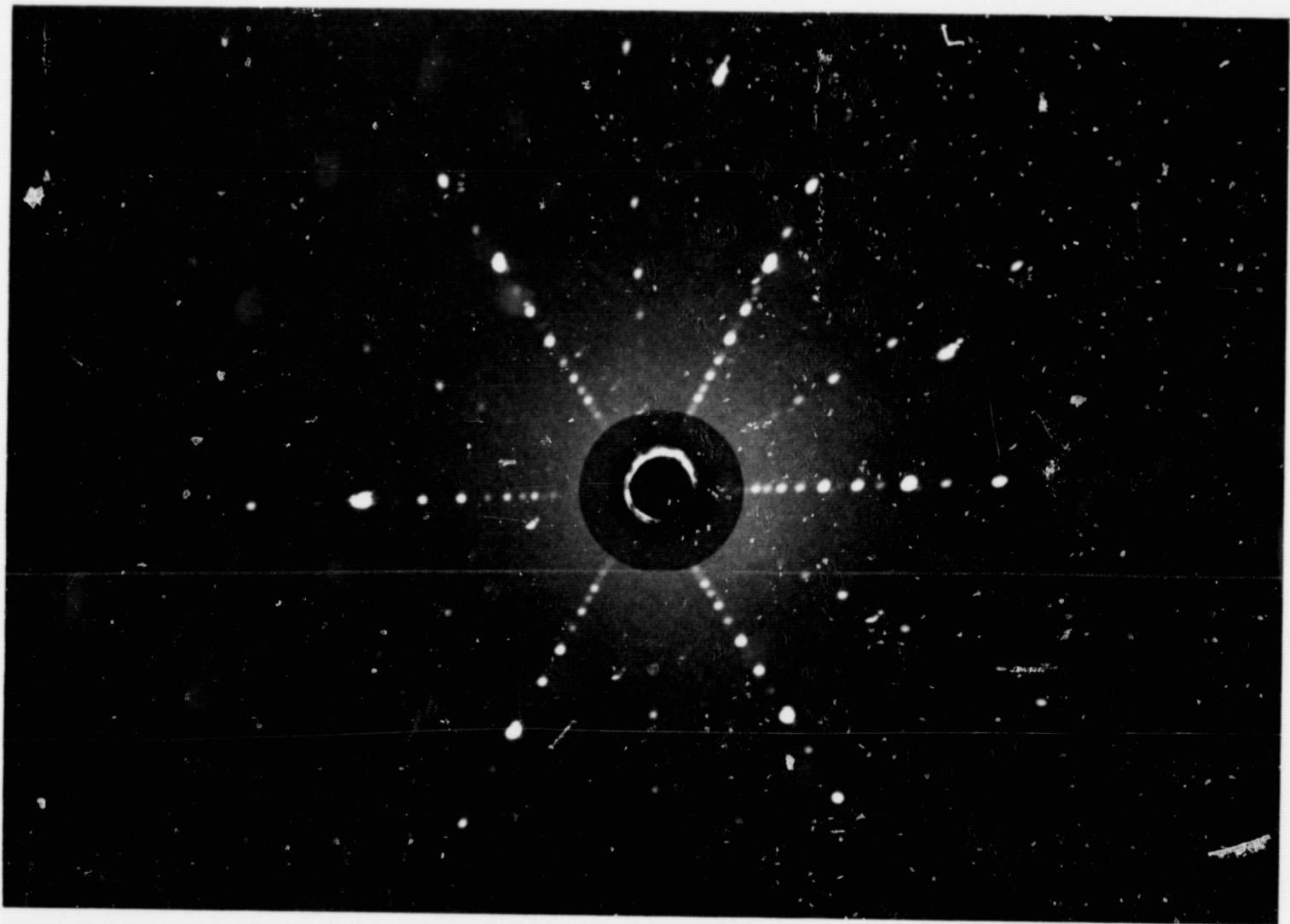


Figure 2. Laue Back-Reflection X-Ray Film Print of Grain #1



005398

Figure 3. Laue Back-Reflection X-Ray Film Print of Grain #6

2.2 TUNGSTEN ALLOY ELECTRODE MATERIALS

The tungsten alloy electrodes have been electron-beam welded onto tungsten envelopes which were previously brazed onto molybdenum baseplates. The samples are tested in the vacuum emission vehicle by generating Schottky plots for the subsequent calculation of effective work functions. The dimensions of the envelope and baseplate support rods were changed from that normally used; therefore, the emitter-collector spacing at temperature was also changed. The spacing was determined as a function of temperature by inserting various tungsten shims of precisely known thickness between the emitter and collector. As the temperature was raised, the emitter assembly expanded toward the collector, and, when the electrodes were electrically shorted through the shim, the spacing was known at that particular temperature. Each experimental point was repeated 10 times with a reproducibility in temperature of three to four degrees at the shorted condition.

Figures 4 through 10 are Schottky plots of various tungsten alloy electrodes. Table IV corresponds to the Schottky plots, summarizing the bare work function information for all the alloys.

Each of the samples was fine-polished with alumina A, B, and C. The samples were then high-fired at the temperatures indicated before vacuum emission testing was begun.

Of the samples completed, Table IV shows that the addition of small amounts of iridium produces the highest bare work function. The difference between 1% and 2% iridium is negligible.

Both the 95% W/5% Ta and 99% W/1% Ir samples exhibit a decreasing bare work function with increasing emitter temperature. Since this behavior had not been observed on any prior sample examined in this laboratory,

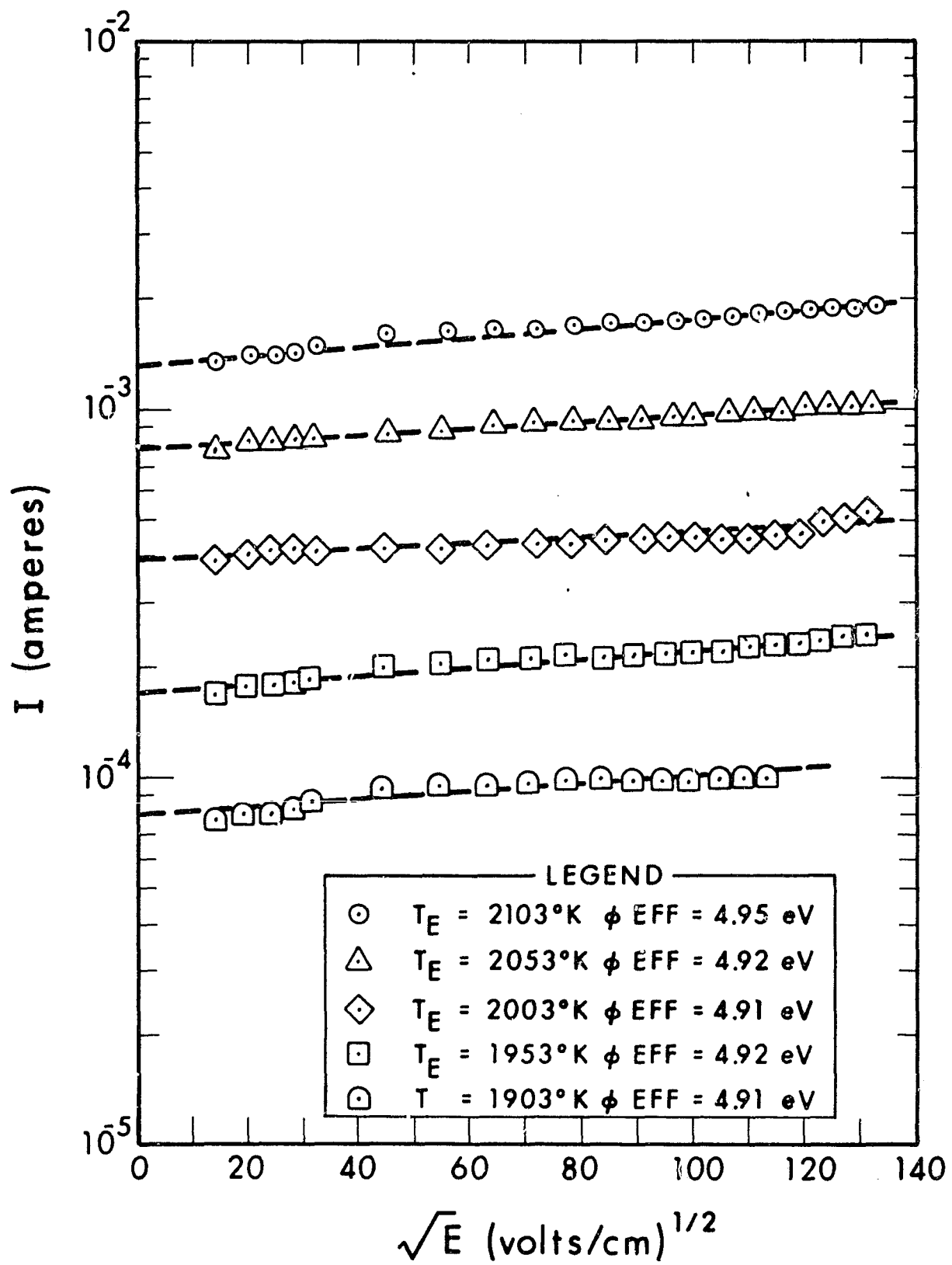


Figure 4. Schottky Plots of 95% W/5% Re from Vacuum Emission Vehicle Measurements (Previously High-Fired at 2373°K for 1 Hour)

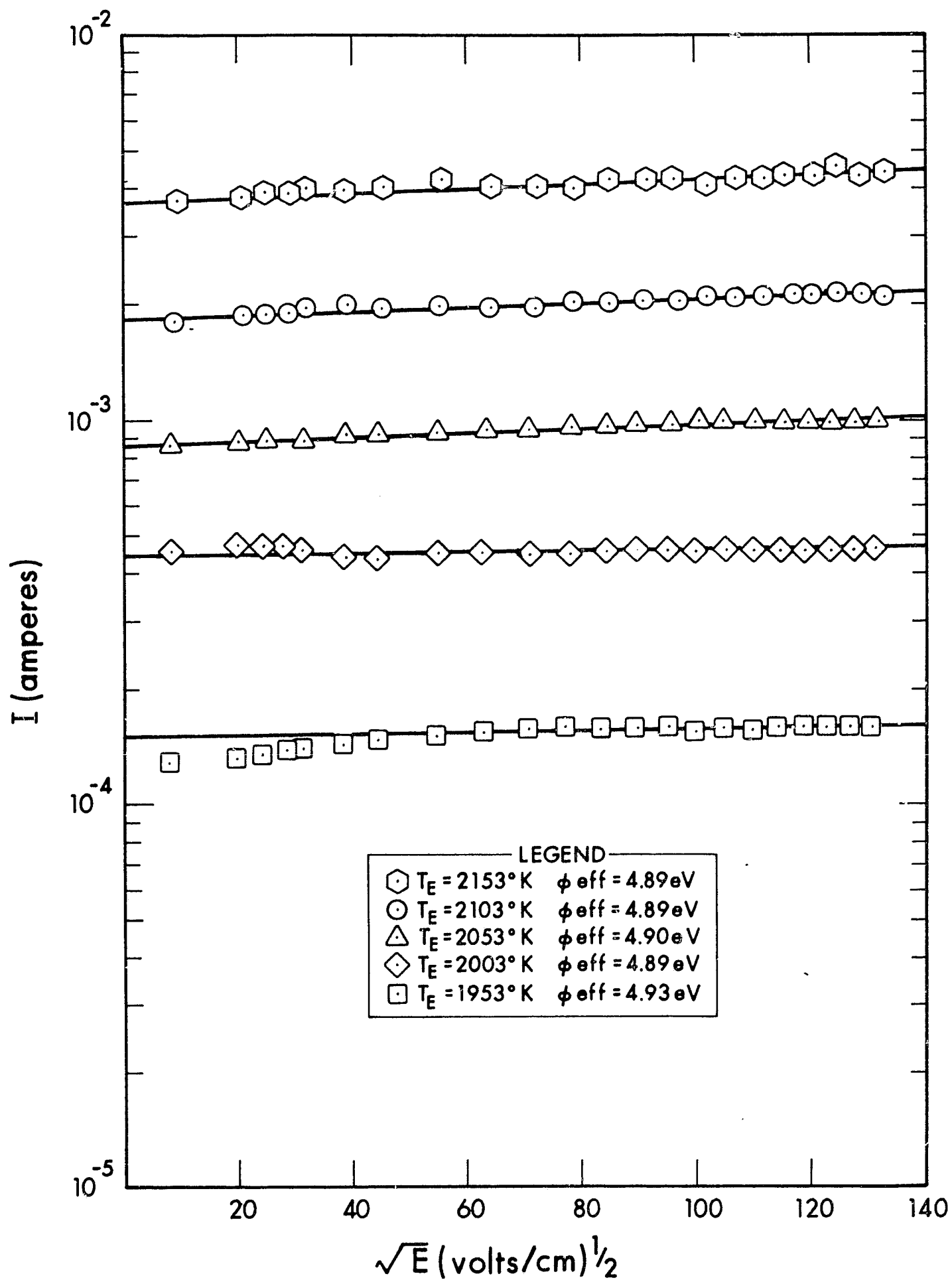


Figure 5. Schottky Plot of 85% W/15% Re From Vacuum Emission Vehicle Measurements (Previously High-Fired at 2373°K for 1 Hour)

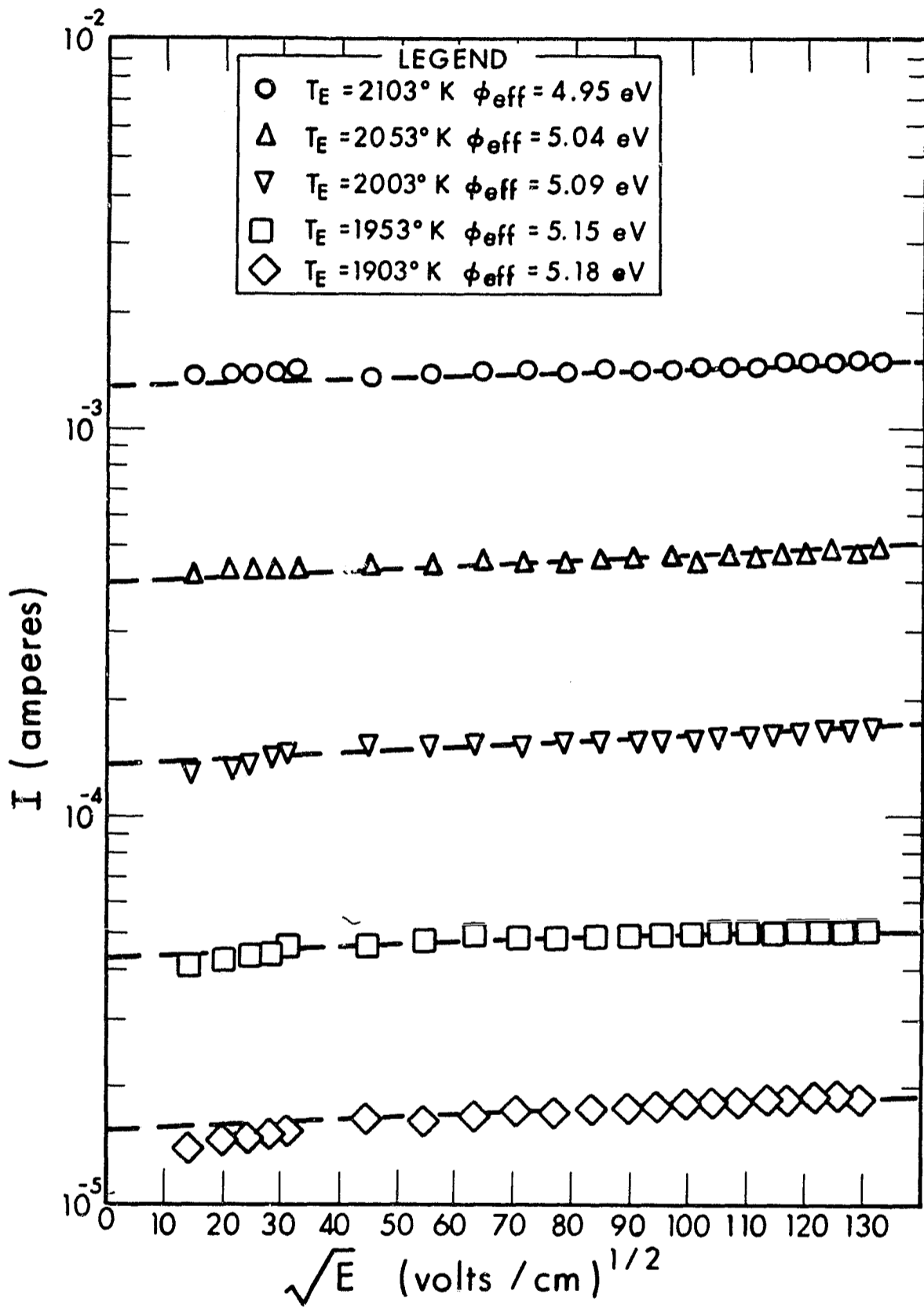


Figure 6. Schottky Plot of 95% W/5% Ta From Vacuum Emission Vehicle Measurements (Previously High-Fired at 2323°K for 1/2 Hour)

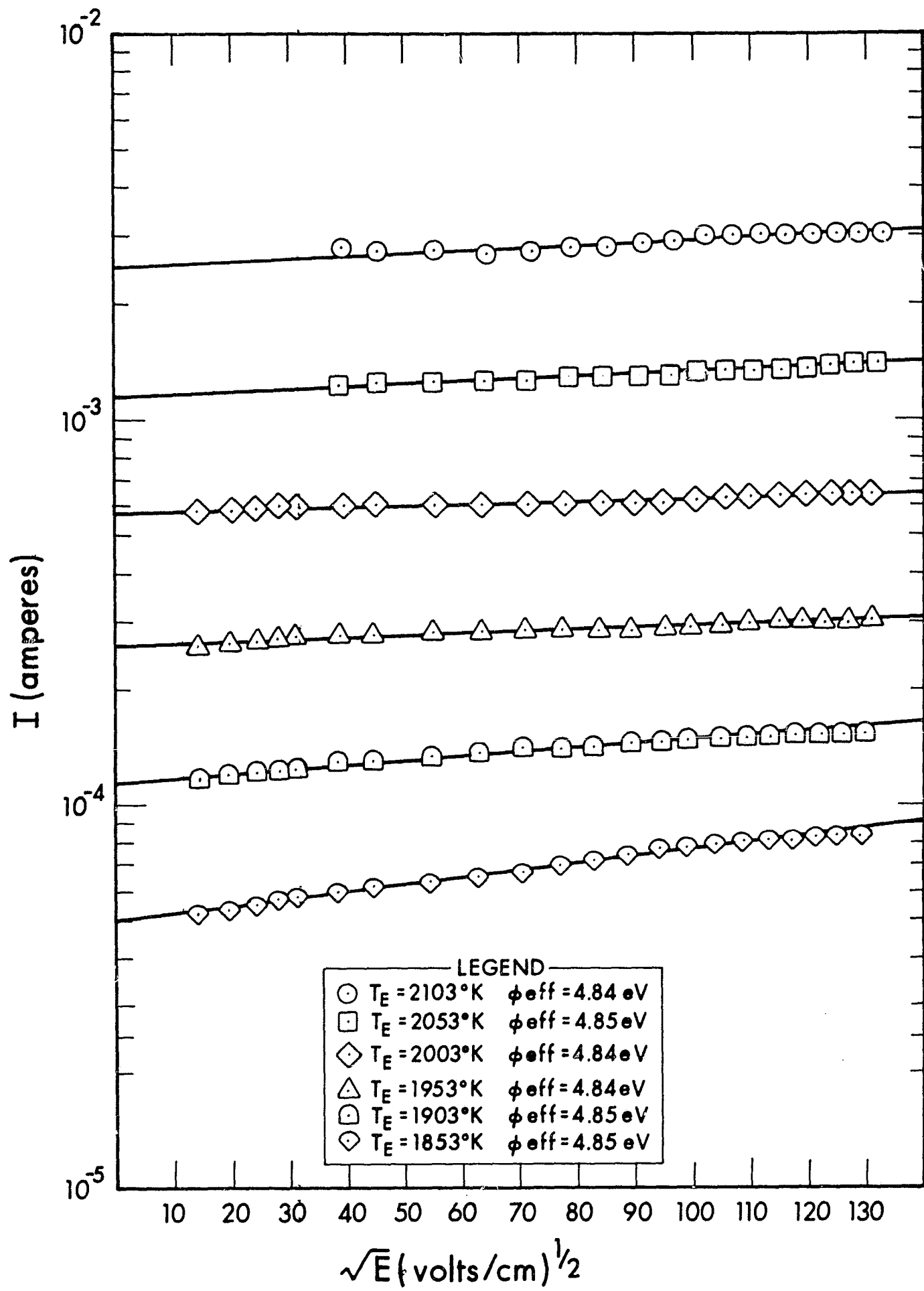


Figure 7. Schottky Plot of 90% W/10% Ta From Vacuum Emission Vehicle Measurements (Previously High-Fired at 2333°K for 1 Hour)

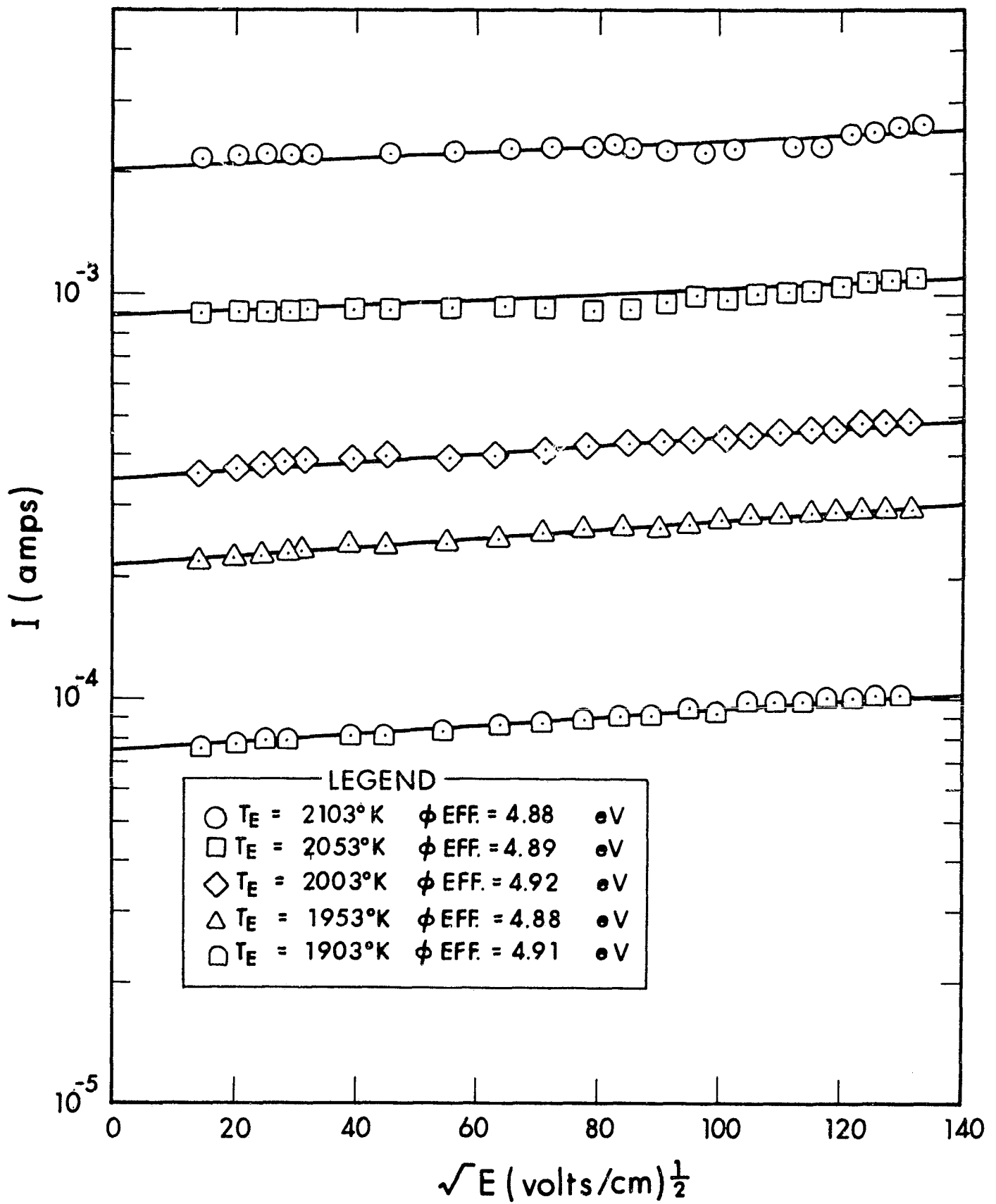


Figure 8. Schottky Plot of 74% W/26% Ta From Vacuum Emission Vehicle Measurements (Previously High-Fired at 2333°K for 1 Hour)

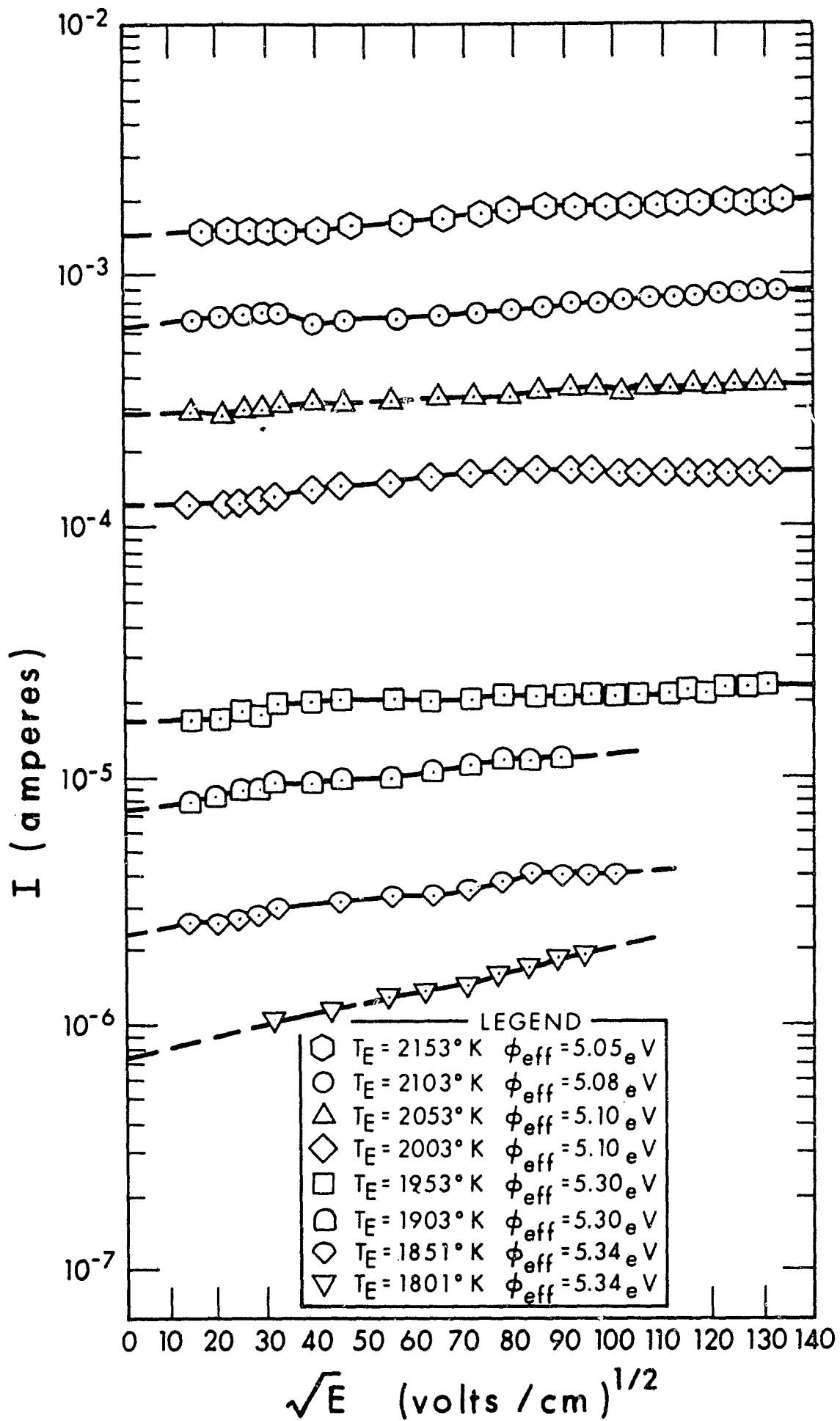


Figure 9. Schottky Plots of 99% W/1% Ir From Vacuum Emission Vehicle Measurements (Previously High-Fired at 2123°K for 2.5 Hours)

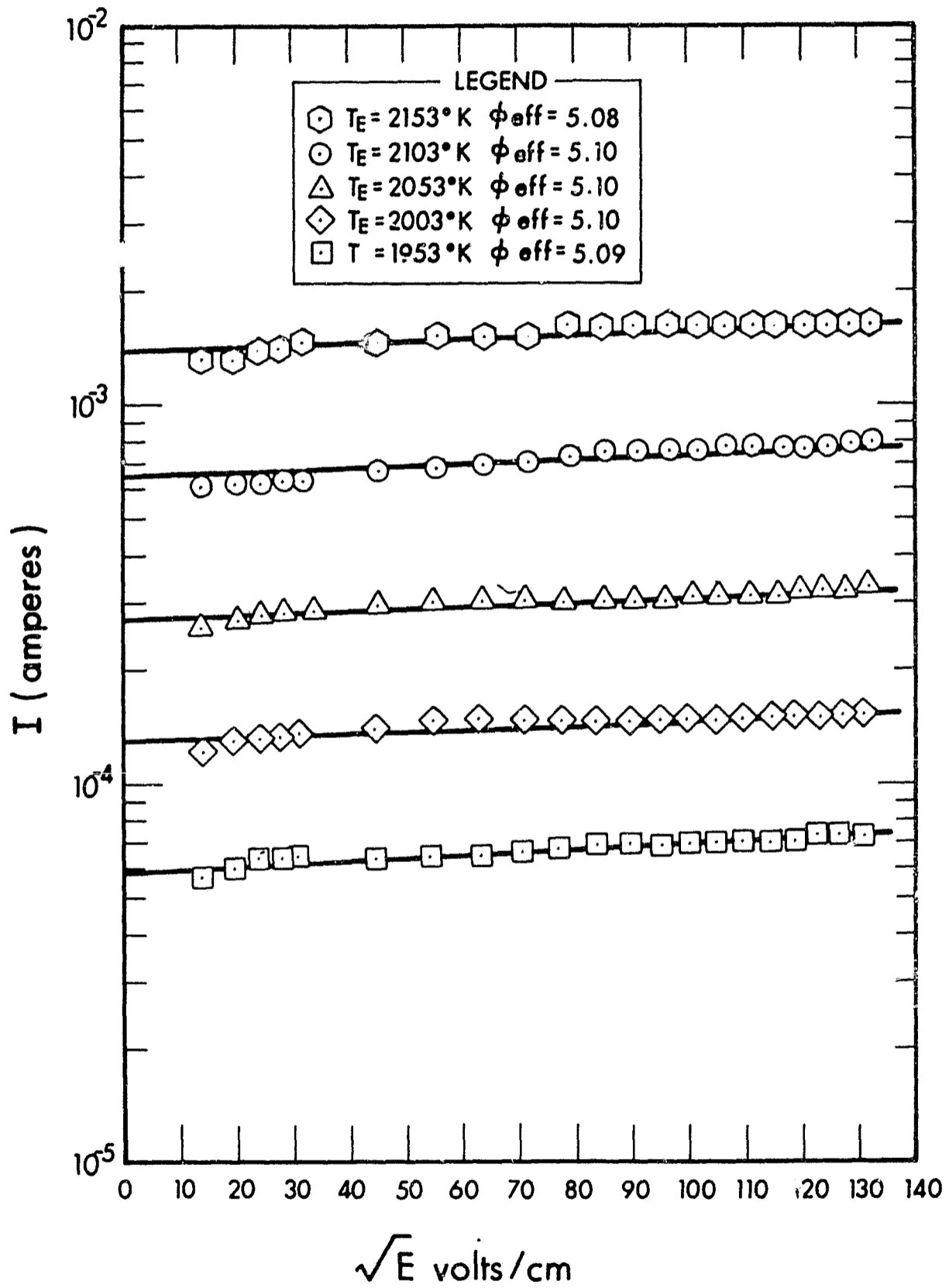


Figure 10. Schottky Plots of 98% W/2% Ir From Vacuum Emission Vehicle Measurements (Previously High-Fired at 2323°K for 1/2 Hour)

TABLE IV
EFFECTIVE WORK FUNCTION OF TUNGSTEN ALLOY ELECTRODES
FROM VACUUM EMISSION VEHICLE-GENERATED
SCHOTTKY PLOTS

T °K	ϕ_{eff} (eV)*						
	5% Re	15% Re	5% Ta	10% Ta	26% Ta	1% Ir	2% Ir
2153	-	4.89	-	-	-	5.05	5.08
2103	4.95	4.89	4.95	4.84	4.88	5.08	5.10
2053	4.92	4.90	5.04	4.85	4.89	5.10	5.10
2003	4.91	4.89	5.09	4.84	4.92	5.10	5.10
1953	4.92	4.93	5.15	4.84	4.88	5.30	5.09
1903	4.91	-	5.18	4.85	4.91	5.30	-
1853	-	-	-	4.85	-	5.34	-
1801	-	-	-	-	-	5.37	-

* Experimental error ± 0.04 eV

special care was taken to recheck all the data. A polycrystalline molybdenum sample previously examined was rerun occasionally to verify the reproducibility of the measuring system. It was found on each occasion to be unchanging. The 99% W/1% Ir sample was held at 1903°F for 5 hours. The Schottky plot was checked at 100, 300, 500, 700 and 900 volts once an hour and the emission was found to be independent of time at temperature.

Although the emission properties of the samples do not appear to be time dependent, the behavior may be due to the dispensing action of the solute atoms (Ir) from the bulk material (W). Since the percentage of solute atoms is very small, at high temperatures they may be

evaporated from the surface at a higher rate than they are replenished from the bulk.

The rhenium samples and the tungsten samples show an increase in work function as the relative amount of solute is decreased except for the 26% Ta sample. The 5% Ta sample exhibits a work function higher than that for 5% Re, which is somewhat unexpected.

Figures 11 through 21 are thermionic emission microscope mosaics of the various wrought tungsten alloy electrodes. The material was supplied by Battelle Memorial Institute.

Of all the mosaics, pure tungsten has the largest grain size. As the addition of a second phase increases, the grain size decreases. In Fig. 12, the 5% Re sample shows an intergranular pattern which may be due to twinning, although the exact mechanical treatment of the sample by Battelle is unknown. The 15% Re sample in Fig. 13 does not exhibit this structure. In the 1% Ir mosaic of Fig. 17, veins appearing almost as cracks occur randomly in the sample, through grains and across grain boundaries, and are unaccounted for. Dark smudged areas accompany each of the veins. These may be regions of impurities in the sample. After the vacuum emission tests were completed on this sample, deposits were observed on the collector and guard ring corresponding to the same veined and smudged areas on the sample. The 2% Ir mosaic, Fig. 18, also displays two areas of apparent impurities, seen as white spots in the lower center portion of the picture. The 2.5% Os mosaic in Fig. 19 shows some variation in grain size, and the 5% Os mosaic in Fig. 20 shows a high degree of grain size variation and segregation. Figure 20 also shows an apparent area of impurities represented by the bright spot just left of the center of the mosaic.

005546

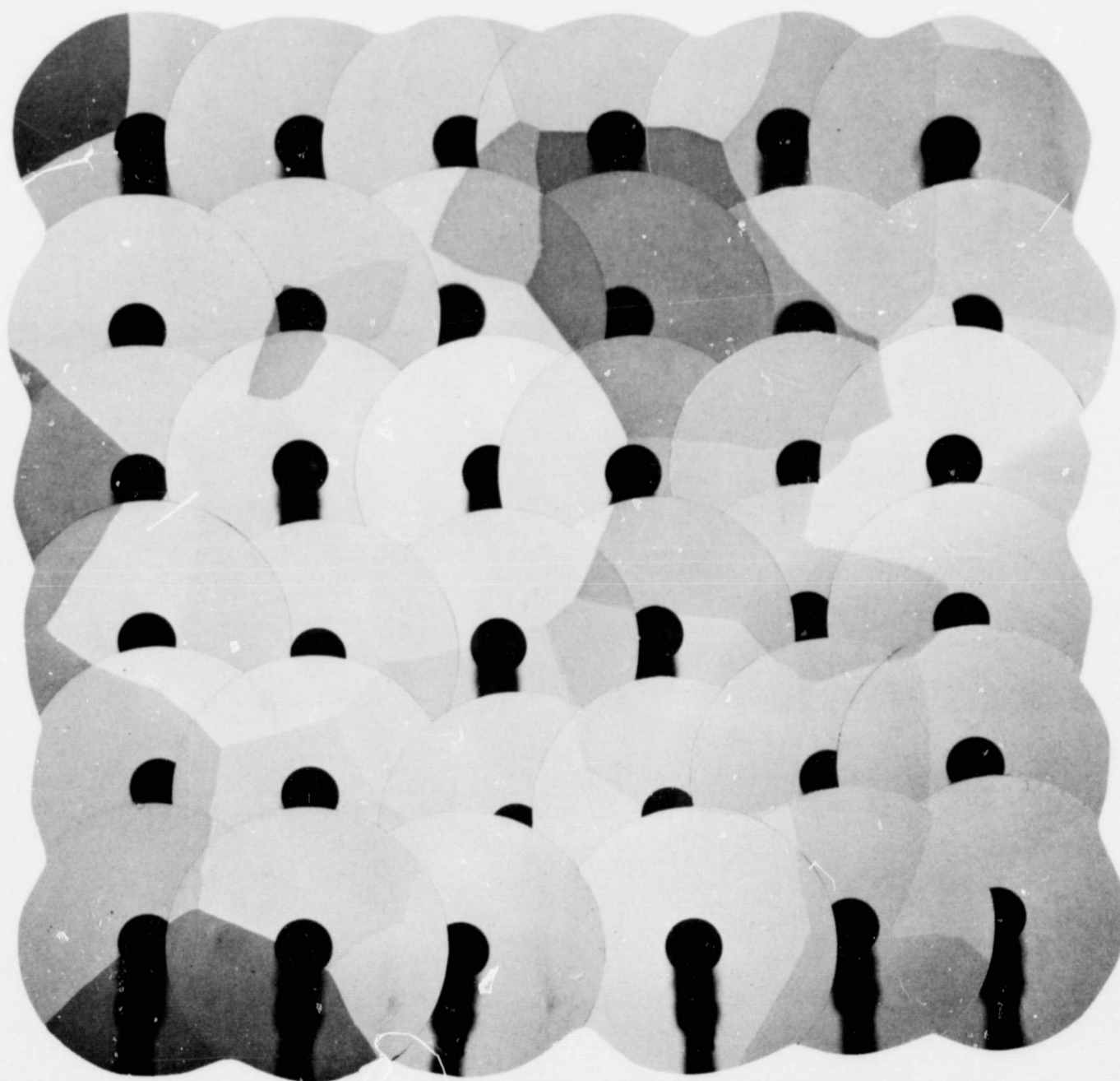
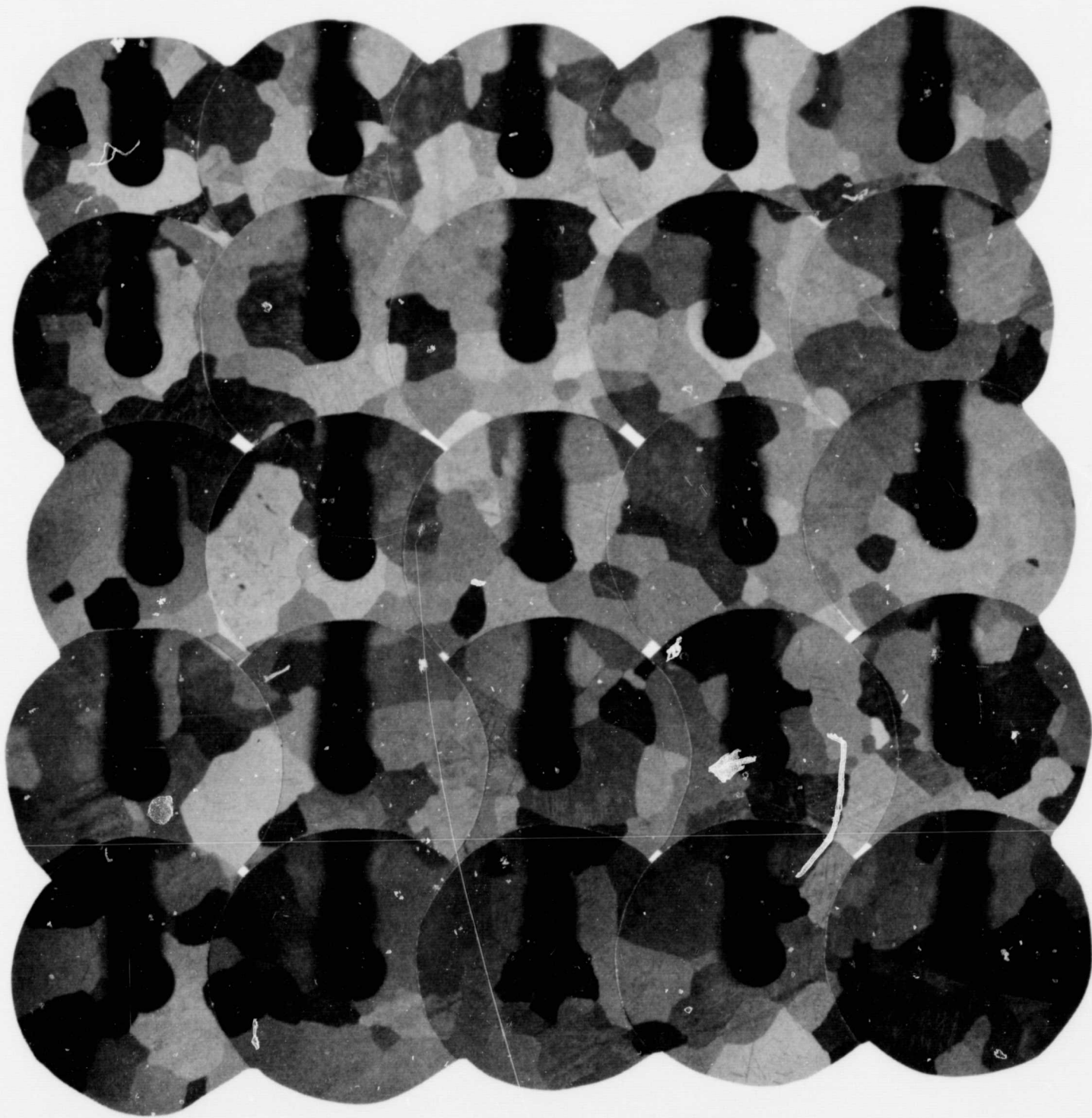
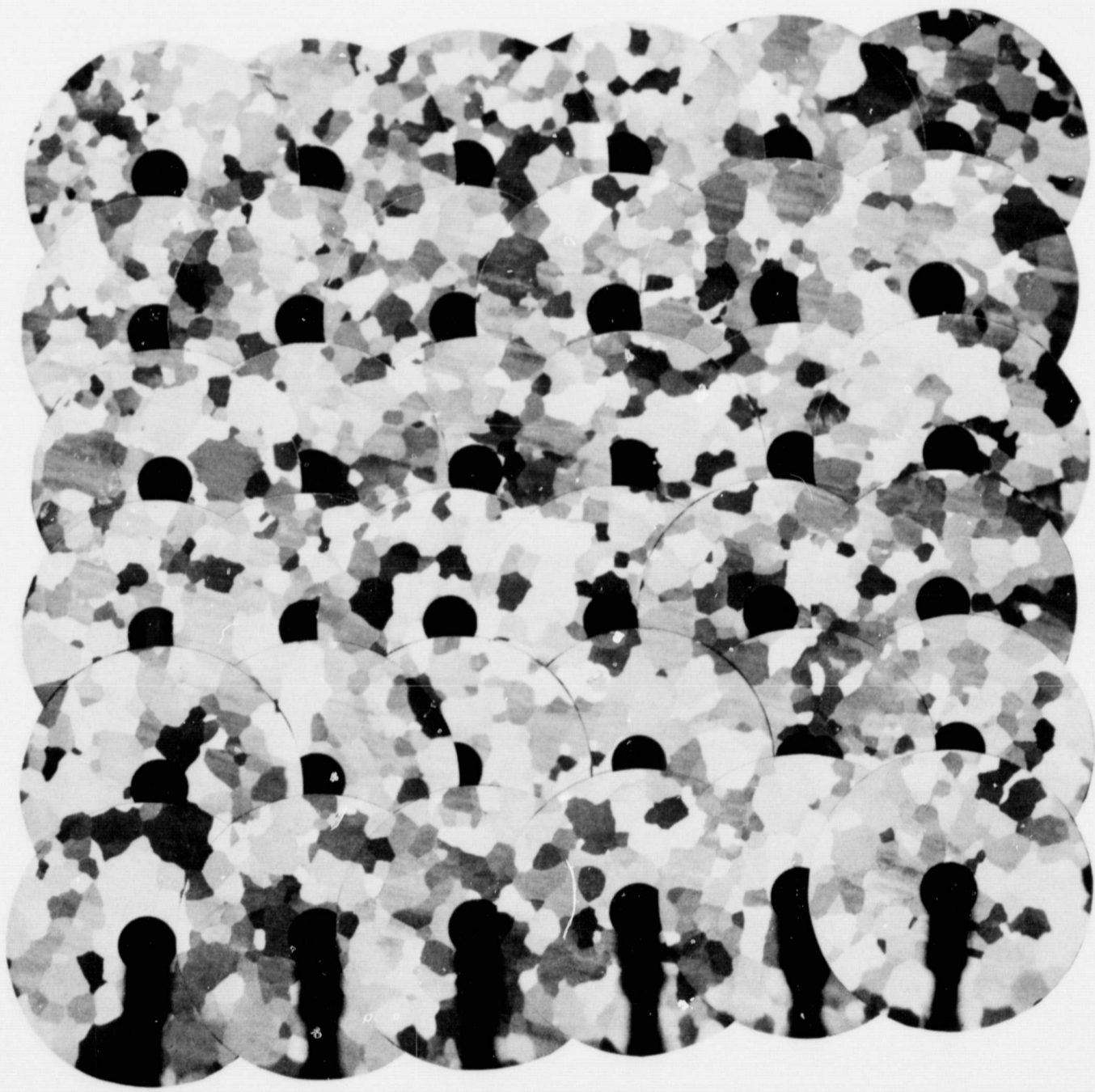


Figure 11. Thermionic Emission Microscope Mosaic of Pure Tungsten
(Magnification 42.5; $T_E = 2003^\circ\text{K}$)



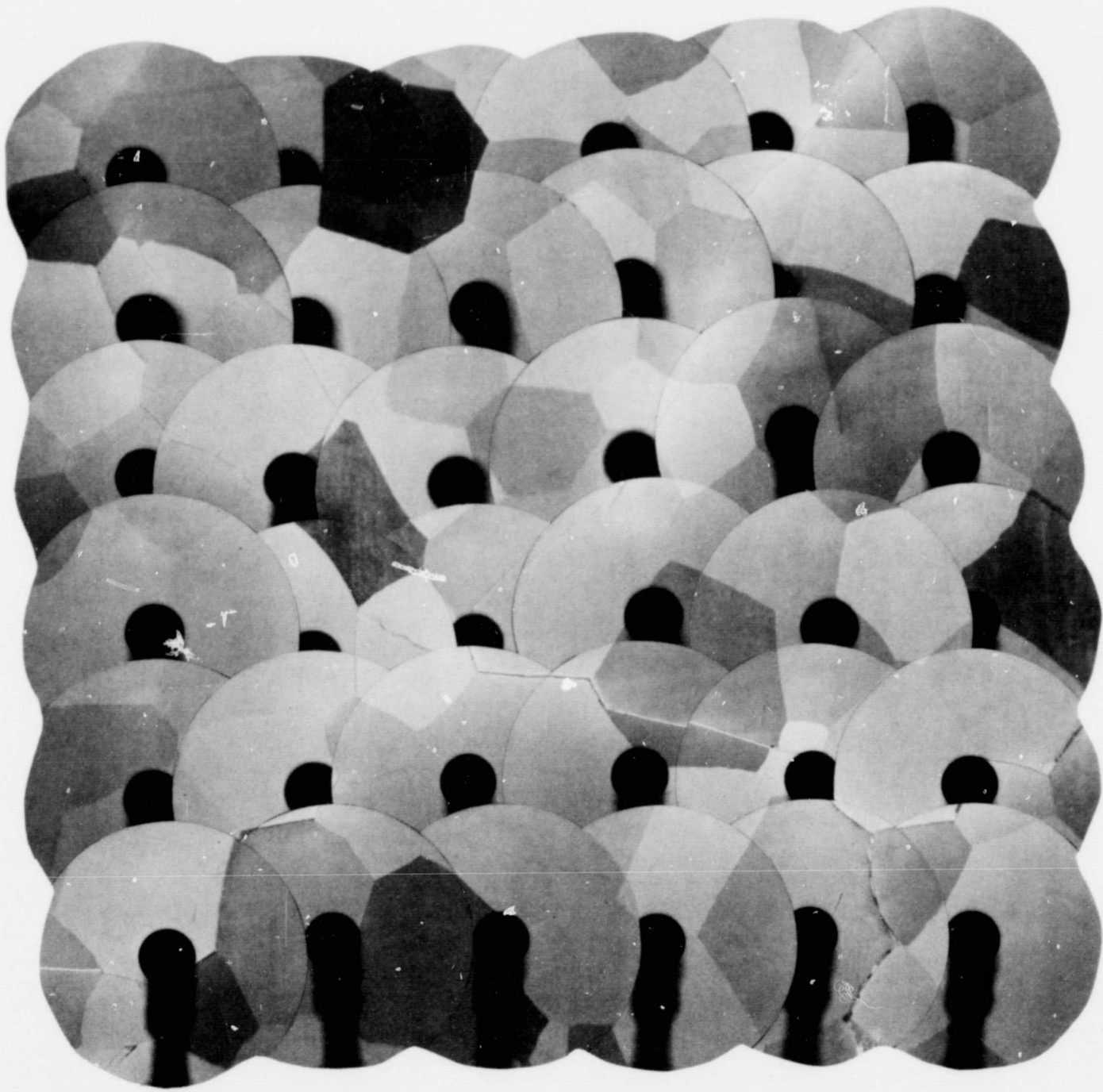
005397

Figure 12. Thermionic Emission Microscope Mosaic of 95% W/5% Re
(Magnification 42.5X; $T_E = 1953^\circ\text{K}$)



005451

Figure 13. Thermionic Emission Microscope Mosaic of 85% W/15% Re
(Magnification 42.5X; $T_E = 2063^{\circ}\text{K}$)



005396

Figure 14. Thermionic Emission Microscope Mosaic of 95% W/5% Ta
(Magnification 42.5X; $T_E = 2003^{\circ}\text{K}$)

005450

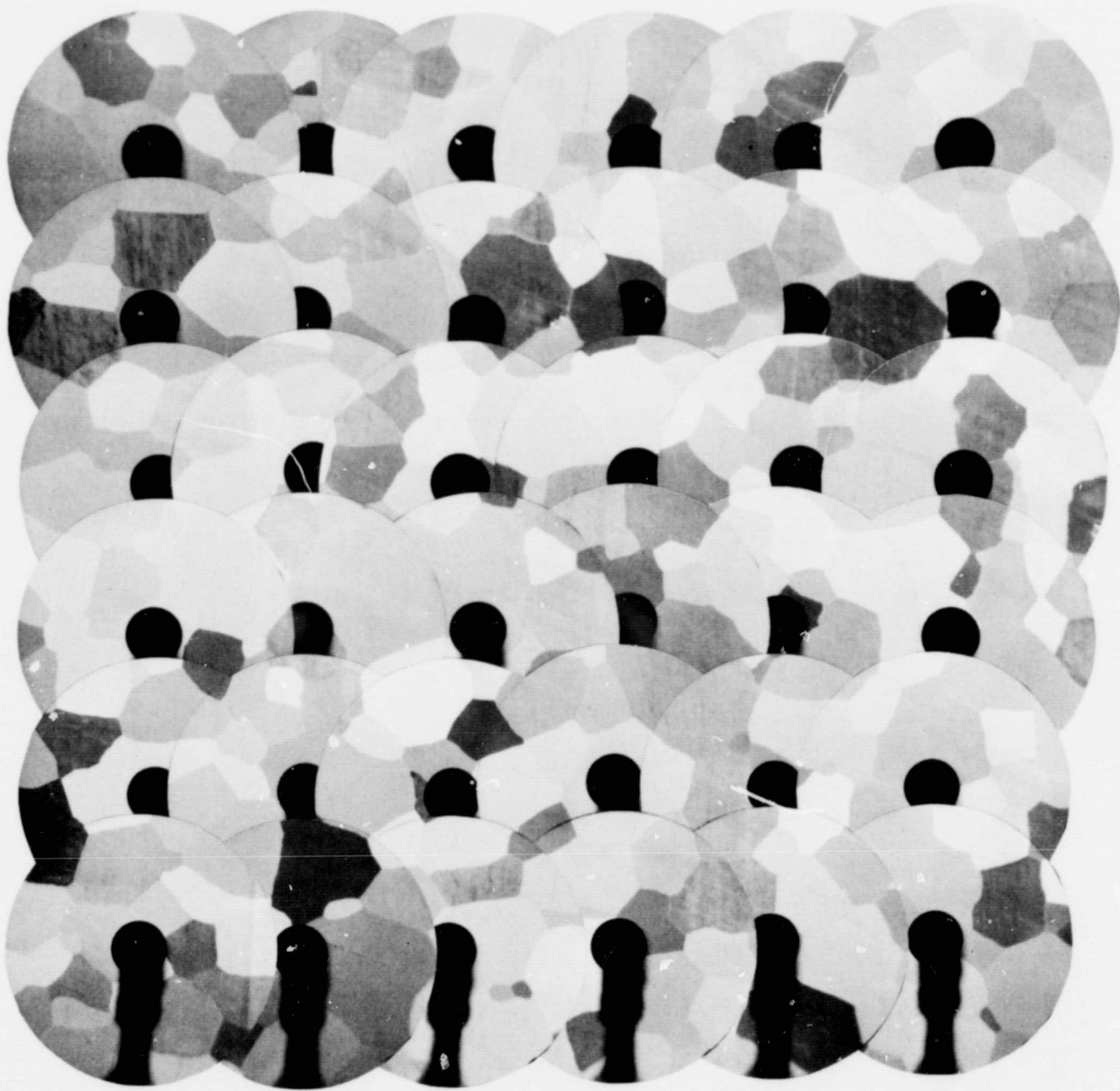


Figure 15. Thermionic Emission Microscope Mosaic of 90% W/10% Ta
(Magnification 42.5X; $T_E = 2053^{\circ}\text{K}$)

005447

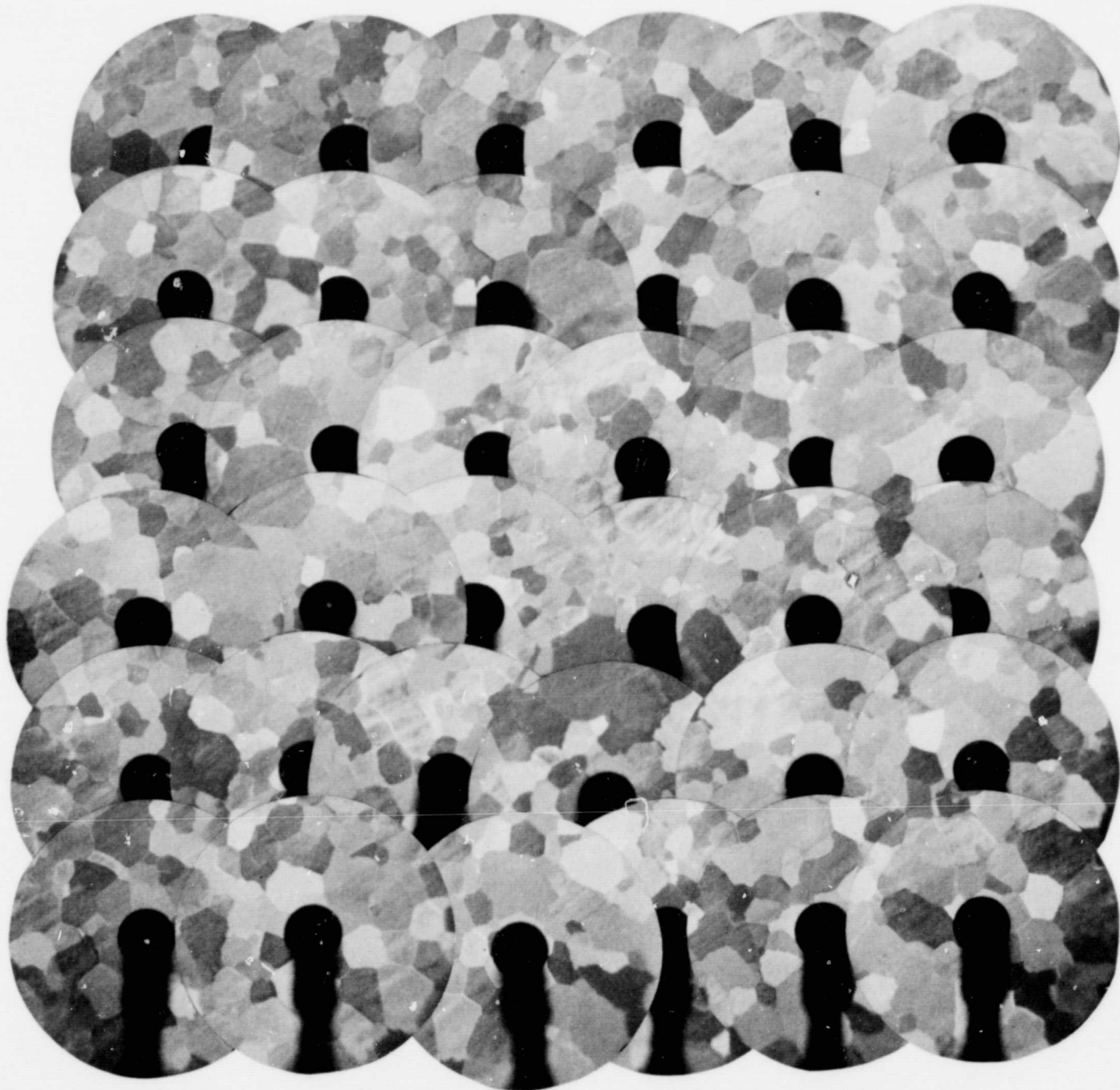


Figure 16. Thermionic Emission Microscope Mosaic of 74% W/26% Ta
(Magnification 42.5X; $T_E = 2003^\circ\text{K}$)

005547

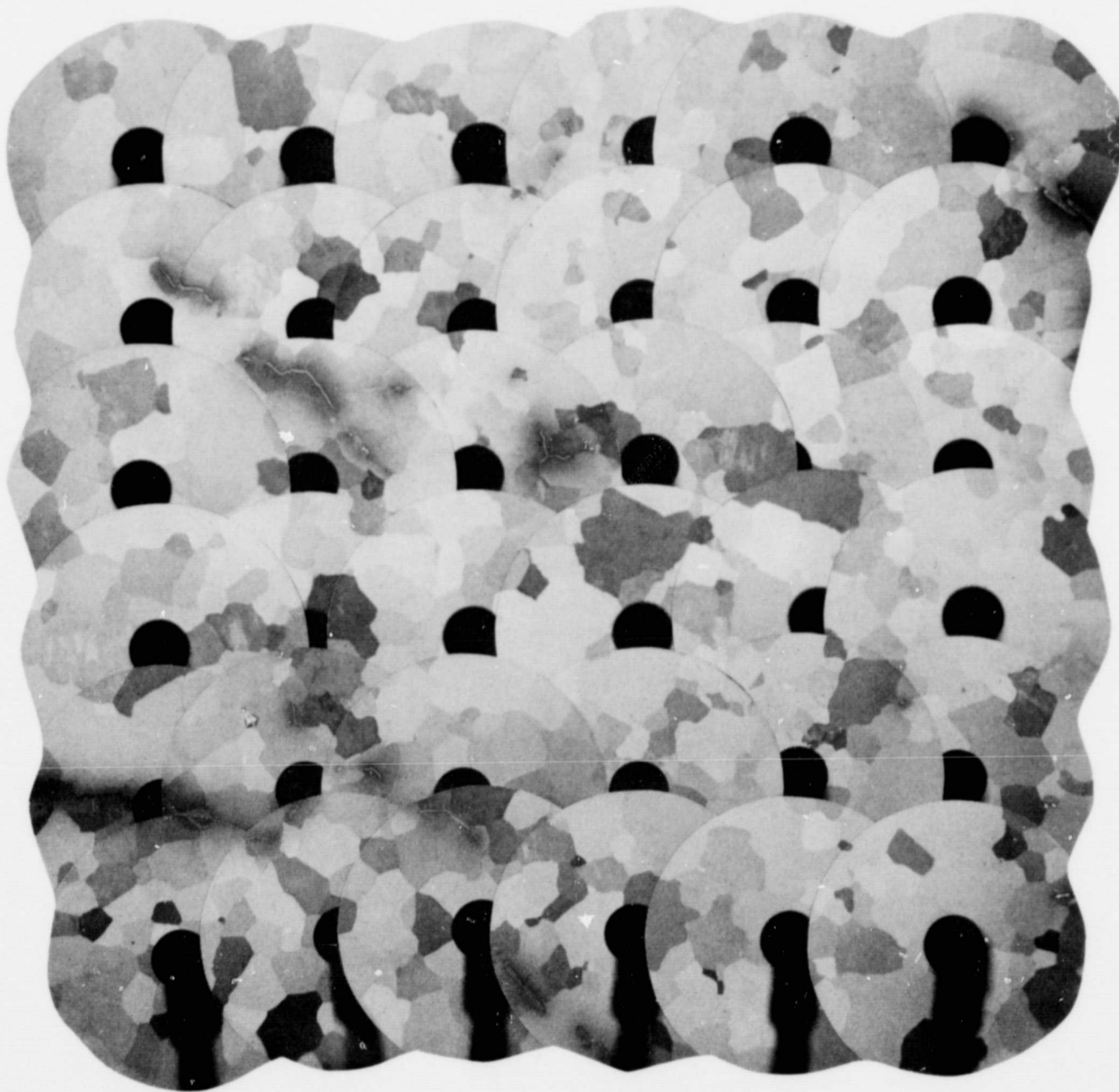
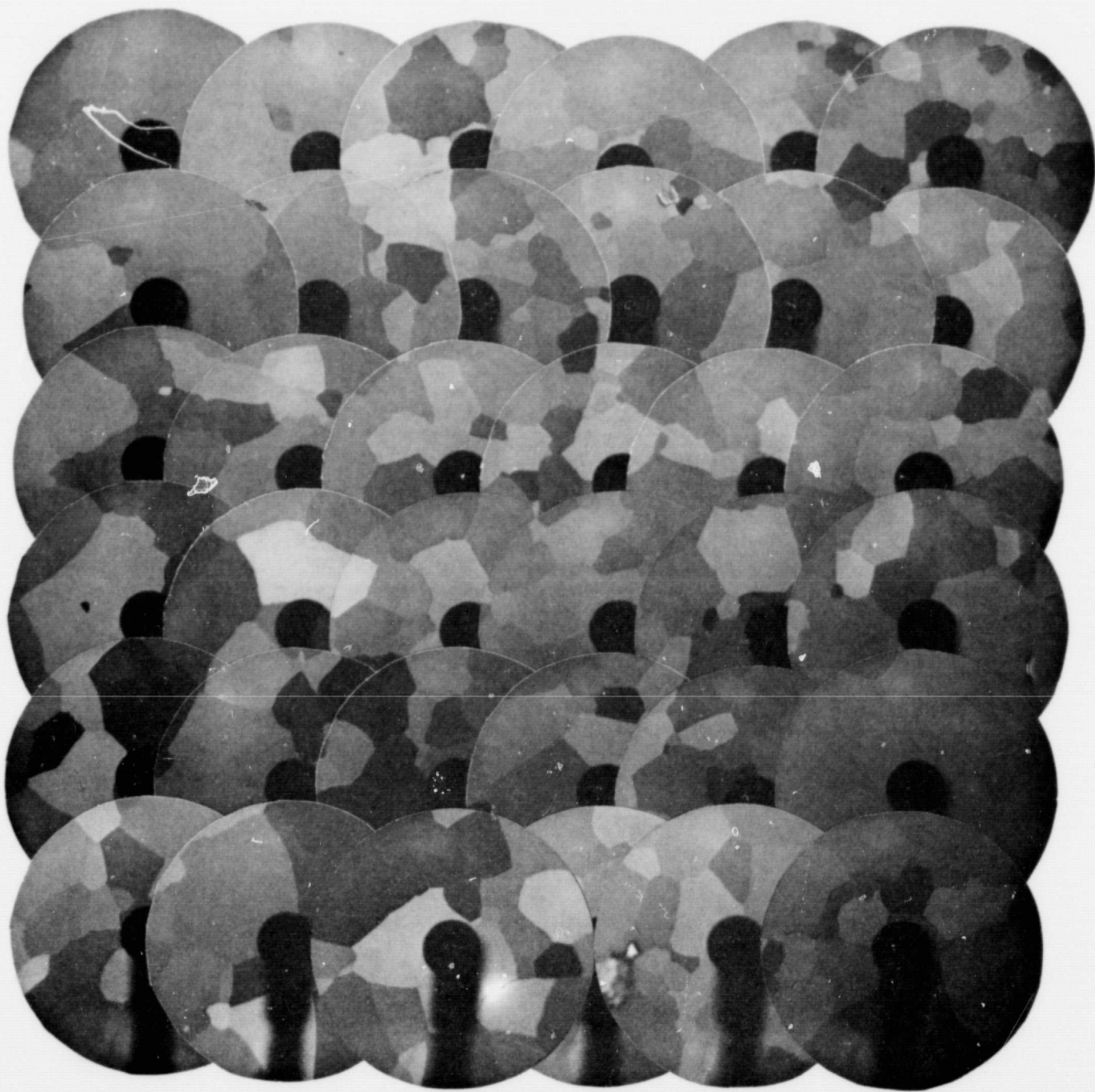


Figure 17. Thermionic Emission Microscope Mosaic of 99% W/1% Ir
(Magnification 42.5; $T_E = 2105^{\circ}\text{K}$)



005452

Figure 18. Thermionic Emission Microscope Mosaic of 98% W/2% Ir
(Magnification 42.5X; $T_E = 2003^\circ\text{K}$)

005448

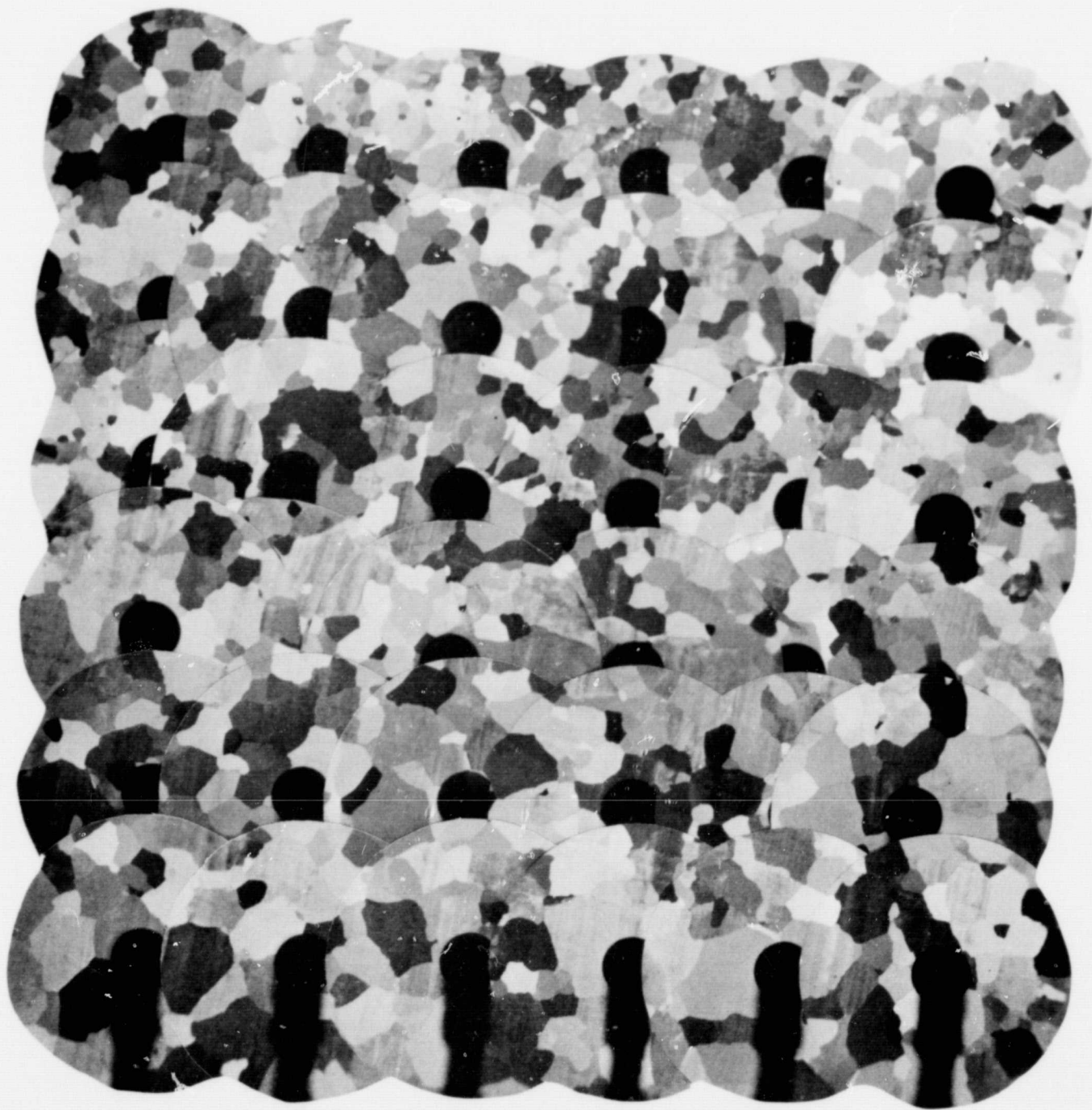


Figure 19. Thermionic Emission Microscope Mosaic of 97.5% W/2.5% Os
(Magnification 42.5X; $T_E = 2053^\circ\text{K}$)

005449

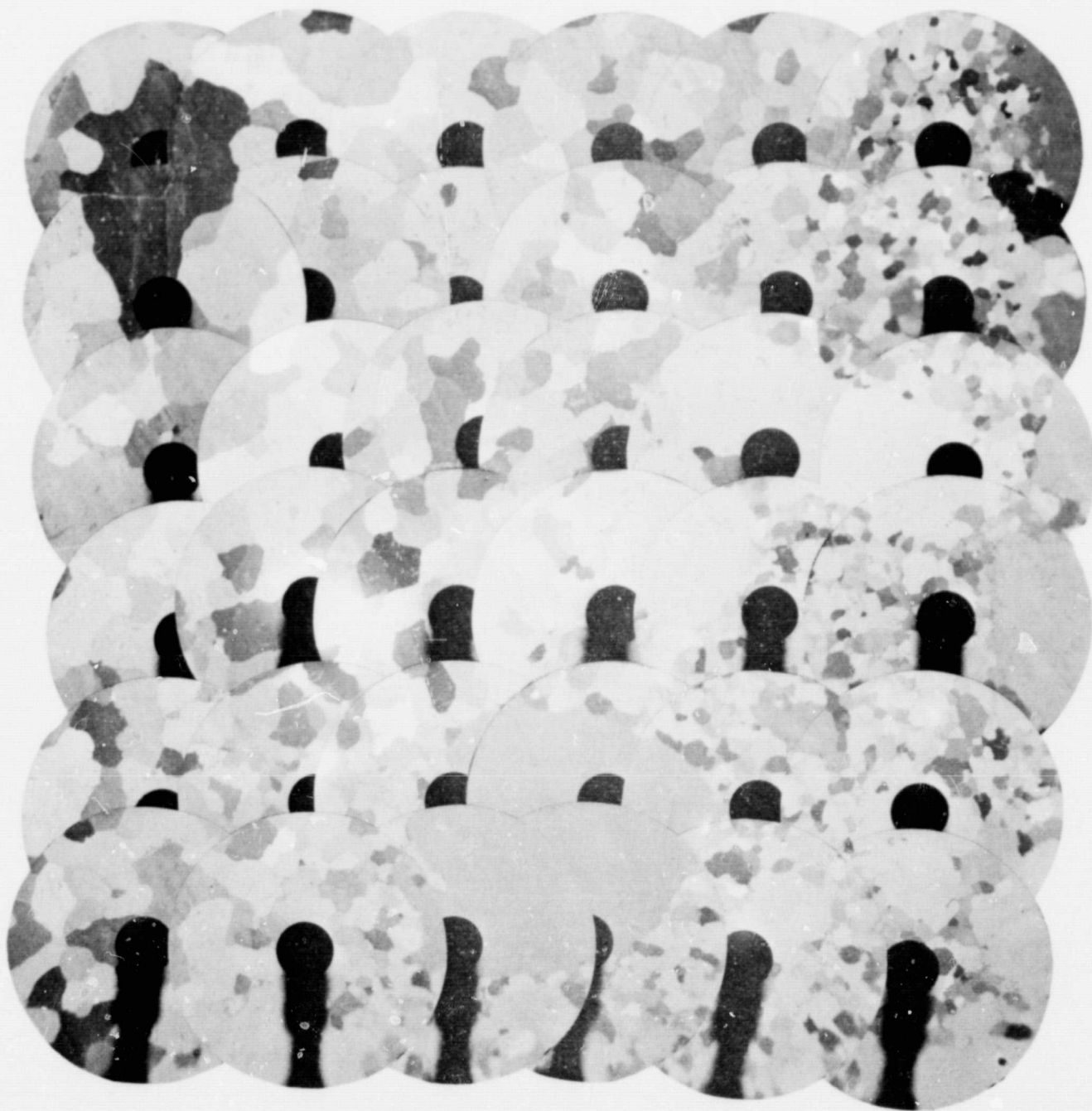


Figure 20. Thermionic Emission Microscope Mosaic of 95% W/5% Os
(Magnification 42.5X; $T_E = 2076^\circ\text{K}$)

SECTION 3

ELECTRODE MATERIALS INVESTIGATION (TASK II)

3.1 VACUUM EMISSION VEHICLE

Six vapor-deposited 22% to 26% rhenium/tungsten samples on wrought 25% rhenium/75% tungsten substrate disks have been examined in the vacuum emission vehicle. Schottky plots are shown in Figs. 21 through 26. Table V gives the accumulated effective work function results.

TABLE V

EFFECTIVE WORK FUNCTIONS OF VAPOR-DEPOSITED
75% W/25% Re ELECTRODE SAMPLES DETERMINED
FROM VACUUM EMISSION VEHICLE MEASUREMENTS

T°K	Effective Work Function* (eV)					
	Sample I	Sample II	Sample III	Sample IV	Sample V	Sample VI
1903	-	-	-	-	4.70	4.82
1953	4.84	4.81	4.79	4.78	4.72	4.85
2003	4.84	4.84	4.81	4.79	4.73	4.86
2053	4.85	4.82	4.81	4.78	4.73	4.88
2103	4.85	4.83	-	4.79	4.74	4.87
2126	-	-	4.82	-	-	-
2153	-	4.84	-	4.76	-	4.86

* Experimental error ± 0.04 (eV)

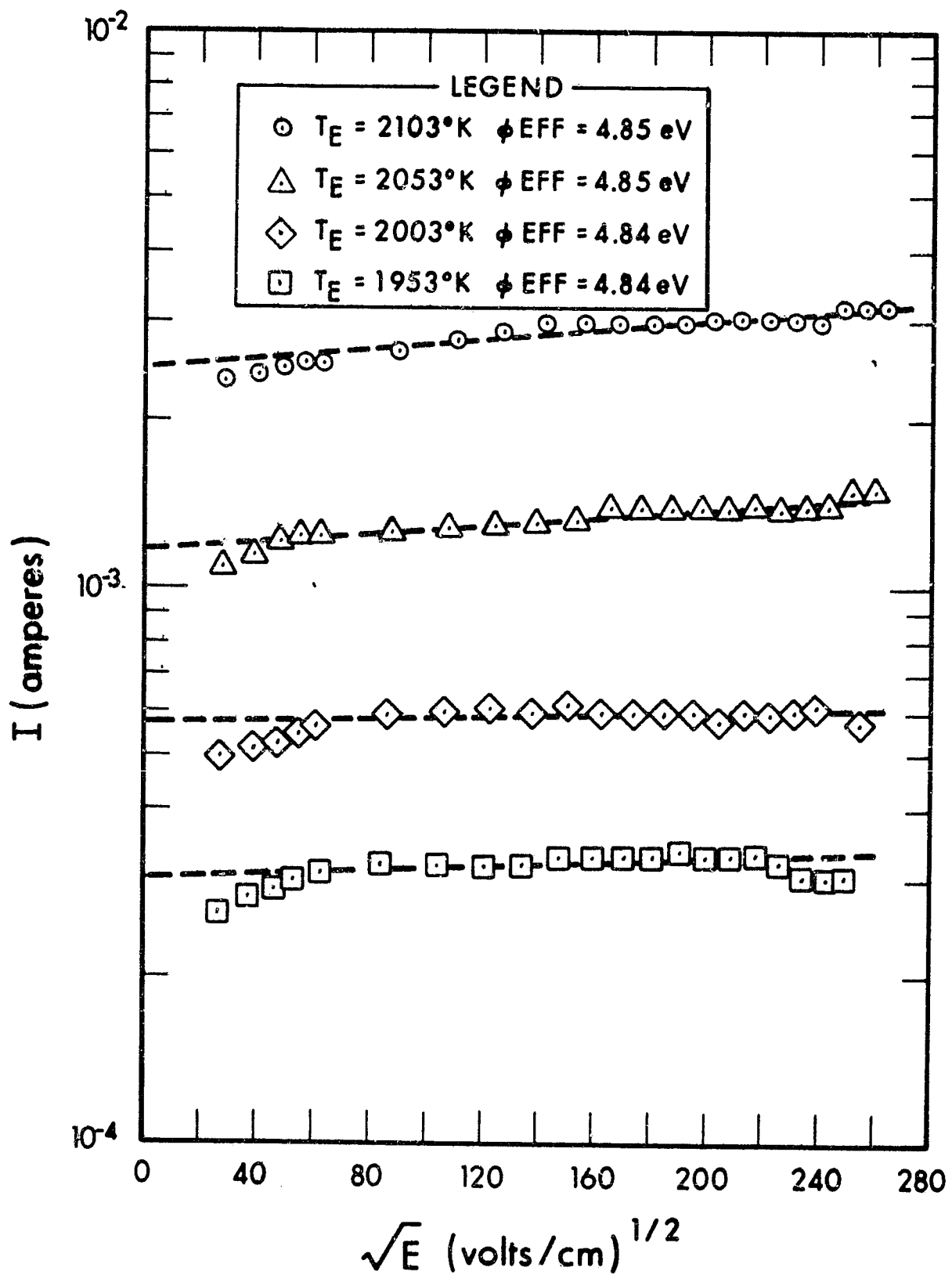


Figure 21. Schottky Plot of 75% Tungsten/25% Rhenium Sample I From Vacuum Emission Vehicle Measurements

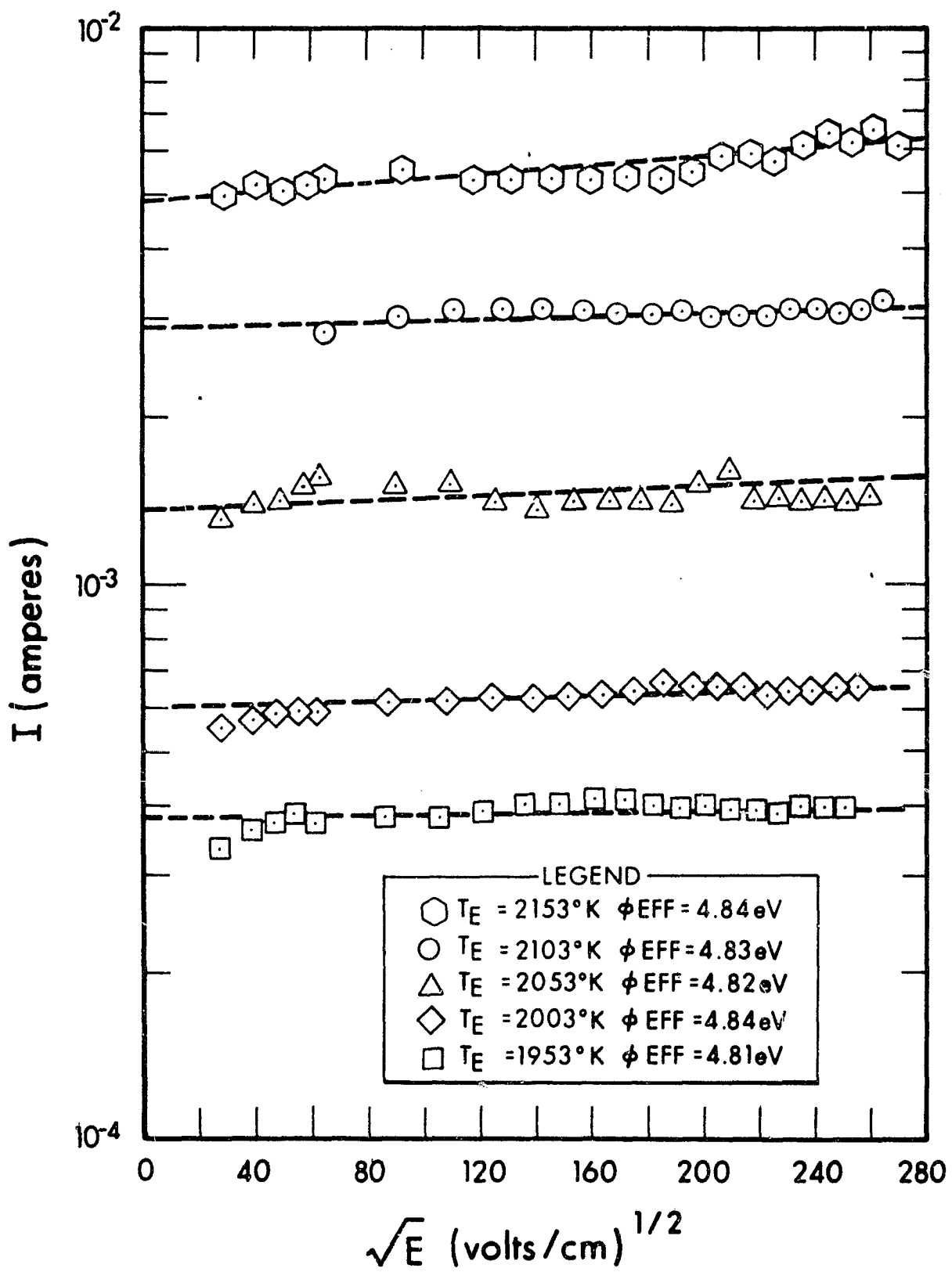


Figure 22. Schottky Plot of 75% Tungsten/25% Rhenium Sample II From Vacuum Emission Vehicle Measurements .

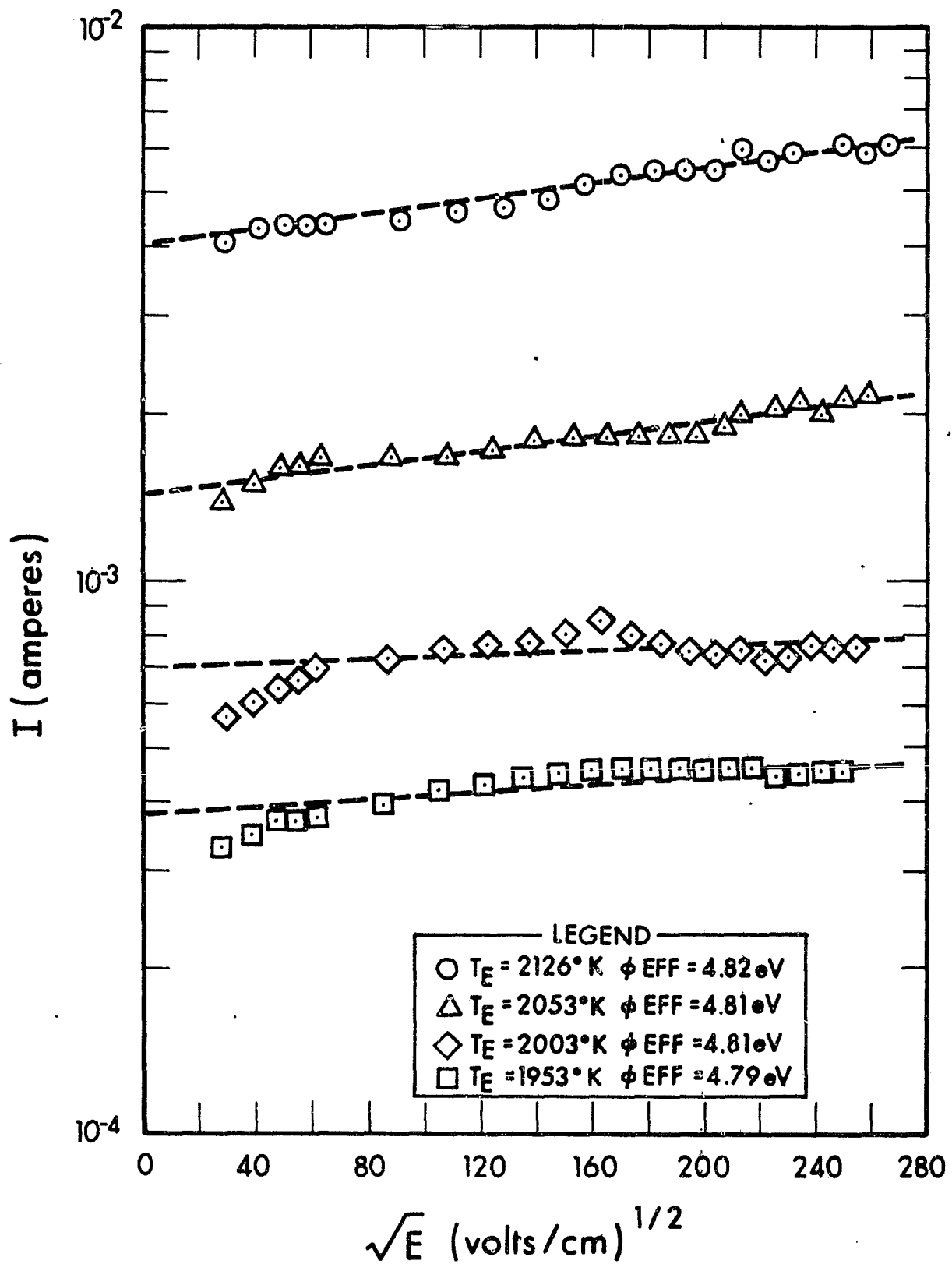


Figure 23. Schottky Plot of 75% Tungsten/25% Rhenium Sample III From Vacuum Emission Vehicle Measurements

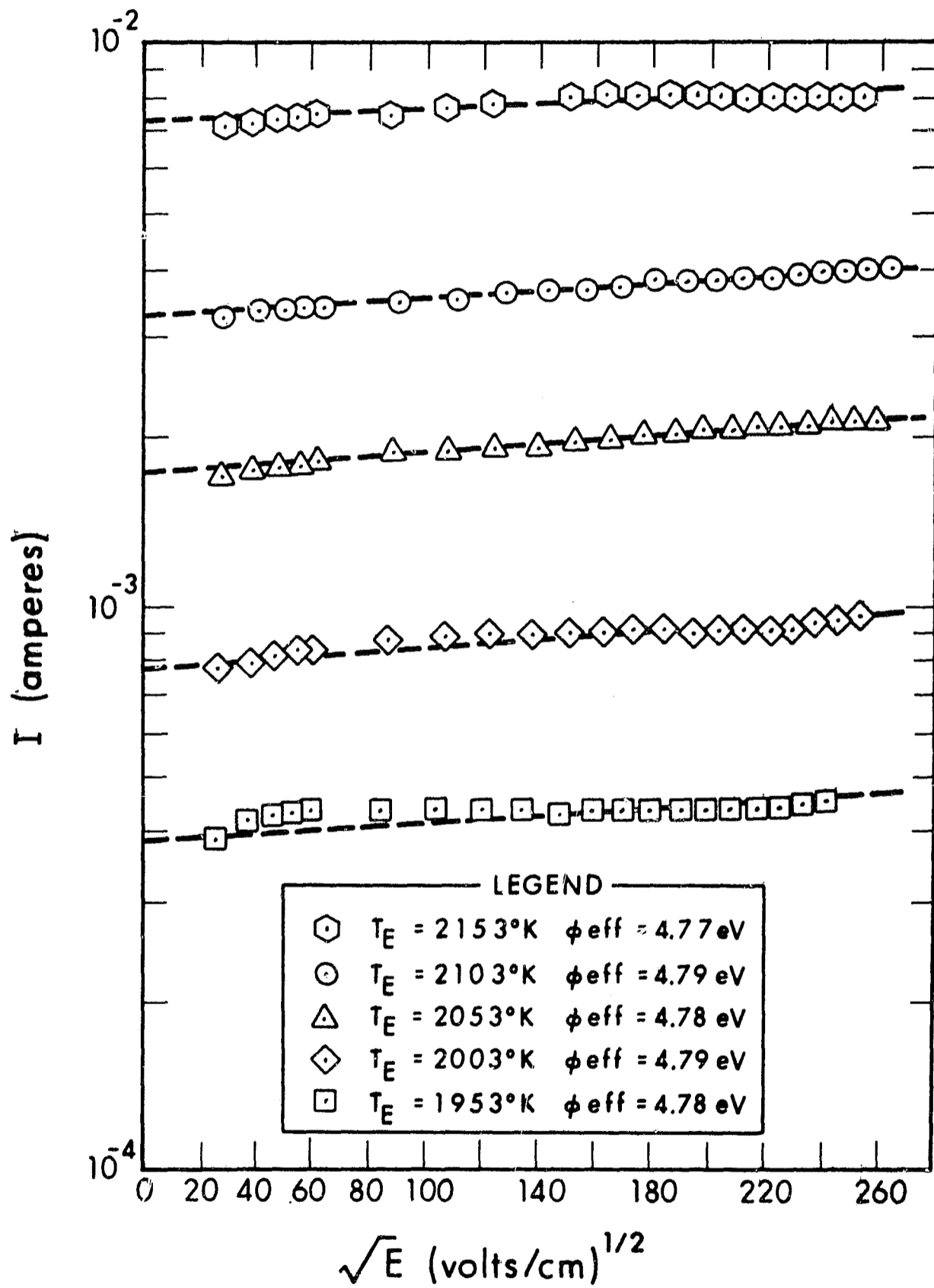


Figure 24. Schottky Plots of CVD 75% W/25% Re Sample IV From Vacuum Emission Vehicle Measurements

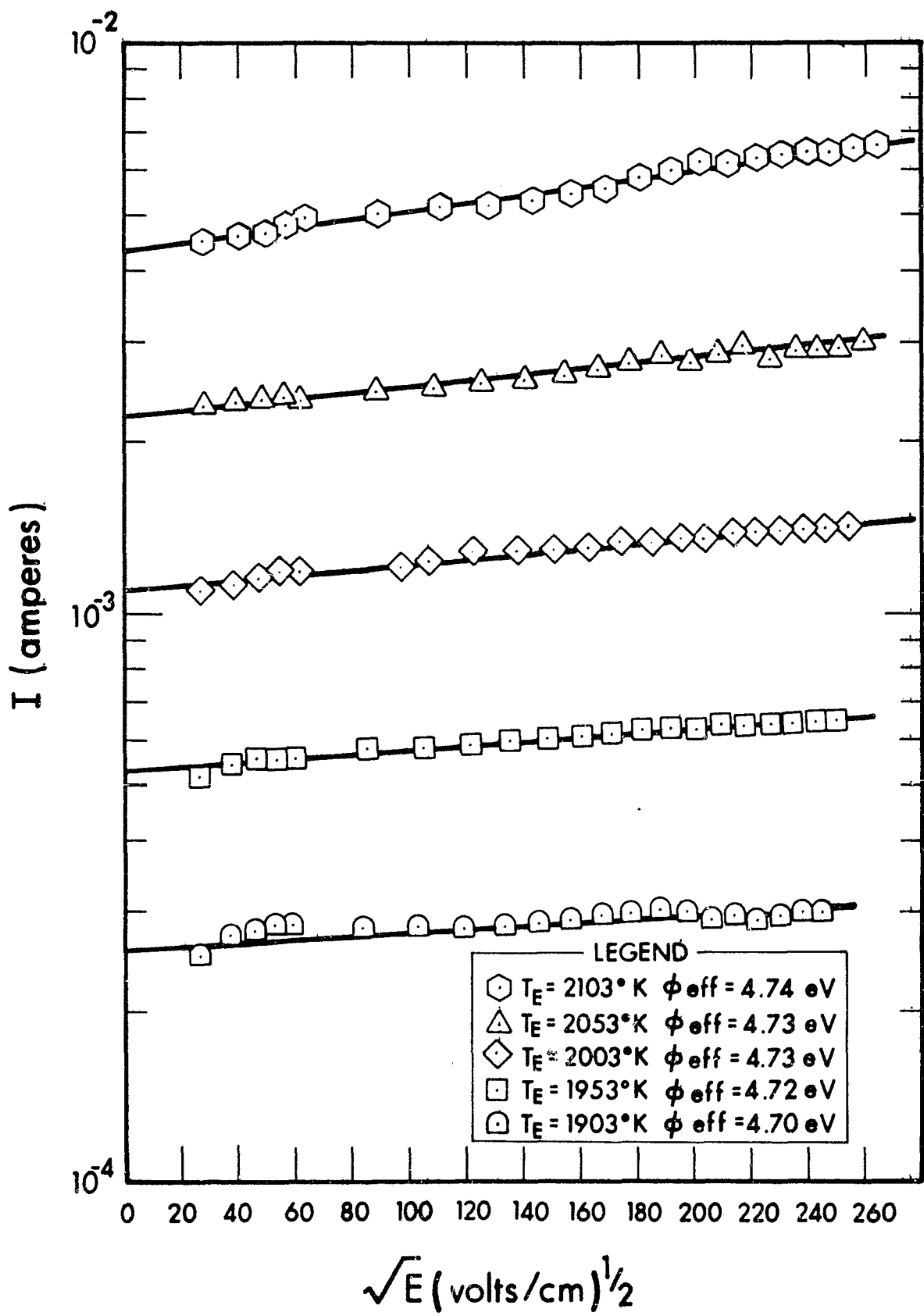


Figure 25. Schottky Plot of CVD 75% W/25% Re Sample V From Vacuum Emission Vehicle Measurements

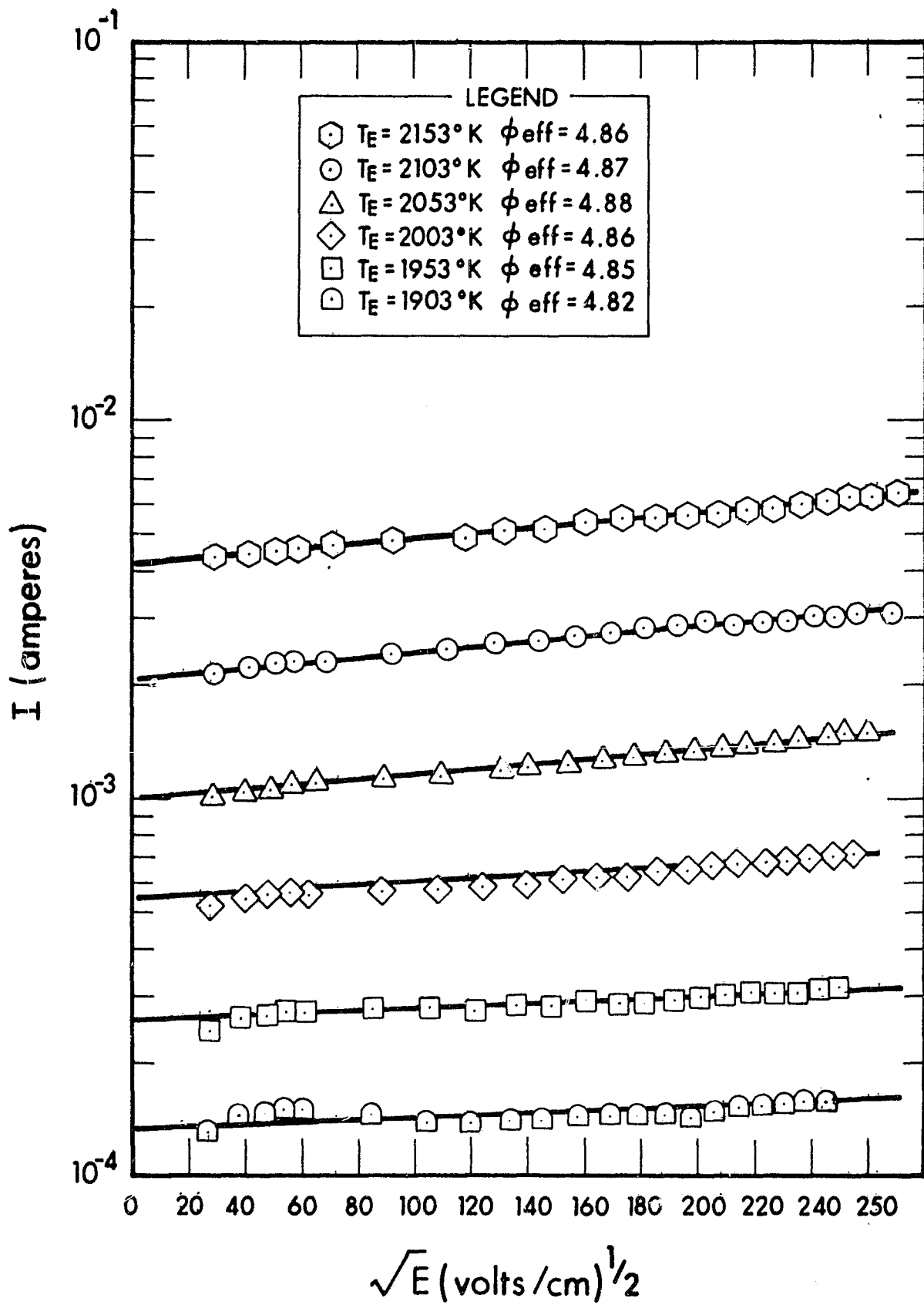


Figure 26. Schottky Plots of CVD 75% W/25% Sample VI From Vacuum Emission Vehicle Measurements

All six samples were high-fired at 2523°K for 1 hour before electron beam welding onto support structures. The samples were then fine-polished with Linde alumina A, B, and C. The samples were again high-fired at 2350°K for 1/2 hour before taking emission measurements. Samples I and II were lightly etched with Murakami's reagent to expose the grain boundaries. The grains appear to be about the same size as vapor-deposited rhenium, i.e., 3 to 10 mils in diameter. Samples I, II, and III were again high-fired at 2350°K for 1/2 hour before the emission measurements were taken.

3.2 THERMIONIC DEVICES

The fabrication of a variable-parameter test vehicle and a planar converter, both employing CVD 75% W/25% Re electrodes are nearing completion. According to the performance information from the variable parameter test vehicle, the operational characteristics for a planar SN 110 type converter will subsequently be selected.

For an emitter, collector, and heat choke of 75% tungsten/25% rhenium, as opposed to pure rhenium (as in some previous EOS devices, Refs. 2 and 3), minor design changes are required. The "optimum" heat choke design requires balancing of the electrical losses with the thermal losses, as given in the equation

$$\alpha = \frac{I^2 \rho \frac{L}{A}}{K\Delta T \left(\frac{A}{L}\right) - \frac{1}{2} I^2 \rho \left(\frac{L}{A}\right)},$$

where I is the total current (in amps) passing through the heat choke, ρ is the electrical resistivity, K is the thermal conductivity, L is the heat choke length, A is the cross-sectional area of the heat choke wall, and ΔT is the temperature drop down the heat choke. Table VI

TABLE VI

HEAT CHOKE ENVELOPE DESIGN PARAMETERS FOR 75% TUNGSTEN/
25% RHENIUM VARIABLE-PARAMETER TEST VEHICLE

L	=	0.400 in.
t	=	0.006 in.
I	=	150 amps
ρ	=	58 $\mu\text{ohm-cm}$ at 1500°K
K	=	0.66 $\frac{\text{watts}}{\text{cm}^{\circ}\text{K}}$
ΔT	=	1000°K
α	=	0.25

summarizes the assumptions made for determining the parameter α for the 75% tungsten/25% rhenium heat choke design. The values of ρ and K are taken from reference 4.

From the values shown in Table VI, calculations show that the thermal power conducted down the heat choke is 62 watts and the joule heating of the heat choke is 6.94 watts. The power radiated by the envelope is approximately 10 watts, so that the total power lost by the emitter down the envelope is 65 watts for an emitter temperature of 2000°K and a current of 150 amps. Since the thermal conductivity of 75% tungsten/25% rhenium is considerably larger than that for rhenium, the heat choke length increases from 0.200 in. for the rhenium system to 0.400 in. for the tungsten/rhenium heat choke. The added length is also necessary to maintain the required length-to-area ratio, since it has been demonstrated by both mechanical and electrical machining processes that the 75% tungsten/25% rhenium envelopes cannot be machined to wall thicknesses much less than 0.007 in. Stresses appear to build up upon machining and the wall buckles and cracks. The added heat choke length can be compensated for in the overall design by increasing the thickness of the collector disk from 0.040 in. to 0.240 in. The envelope

design parameters for the 75% tungsten/25% rhenium electrode planar converter are listed in Table VII. (Values of ρ and K are from Ref. 4.)

TABLE VII

HEAT CHOKE ENVELOPE DESIGN PARAMETERS FOR 75% TUNGSTEN/
25% RHENIUM PLANAR CONVERTER

L	=	0.400 in.
t	=	0.006 in.
I	=	50 amps
ρ	=	58 $\mu\text{ohm-cm}$ at 1500 $^{\circ}\text{K}$
K	=	0.66 $\frac{\text{watts}}{\text{cm}^{\circ}\text{K}}$
ΔT	=	1000 $^{\circ}\text{K}$
α	=	0.036

From the values shown in Table VII, calculations show that the thermal power conducted down the heat choke is 62 watts and the joule heating of the heat choke is 1.11 watts. Allowing 10 watts for radiation, the total power lost by the emitter down the envelope is 71 watts for an emitter temperature of 2000 $^{\circ}\text{K}$ at a current of 50 amps. The parameter α is determined to be 0.036 for a length-to-area ratio of 10.64 cm^{-1} . The linear coefficient of expansion for 75% W/25% Re⁽⁴⁾ at 1000 $^{\circ}\text{C}$ is 5.04 $\frac{\mu\text{in.}}{\text{in.}^{\circ}\text{C}}$ as compared to 6.65 $\frac{\mu\text{in.}}{\text{in.}^{\circ}\text{C}}$ for pure rhenium.

Since the thermal expansion of the tungsten/rhenium alloy is somewhat less than that of pure rhenium, the design for setting the spacing of the planar converter should proceed in the same manner as for previous planar converters.

The 75% tungsten/25% rhenium alloy is brittle at room temperature. Envelope and heat choke piece parts with 7-mil wall thicknesses have been found to be extremely fragile and may be shown to be incapable of withstanding the required handling during normal fabrication processes. Pure rhenium appears to be the best qualified substitute, since the alloy appears to be unacceptable.

SECTION 4
 LOW-TEMPERATURE (1700° - 1800°K) CYLINDRICAL CONVERTER
 (TASK III)

Four cylindrical converters consisting of vapor-deposited rhenium electrodes have been designed and are being fabricated in an iterative manner to provide performance comparison to planar converters of the same electrode materials developed under NASA contract NAS7-514. To provide an exact performance comparison, each converter has an emitter area of 2.0 cm² and a collecting area of 1.88 cm². The four converters are designated SN109CA, SN109CB, SN110CA, and SC110CB.

The cylindrical converters were designed for maximum performance at the interelectrode and emitter temperatures specified in Table VIII.

TABLE VIII
 CYLINDRICAL CONVERTER DESIGN CRITERIA

<u>Converter Designation</u>	<u>Emitter Temperature</u>	<u>Interelectrode Spacing</u>	<u>Power Output</u>
SN109CA, SN109CB	1800°K	0.006 ^{+0.001} / ₋₀₀₀ in.	10.5 W/cm ²
SN110CA, SN110CB	1700°K	0.010 ^{+0.001} / ₋₀₀₀ in.	4.5 W/cm ²

The EOS concept of cylindrical converters is readily adaptable to out-of-pile and radioisotopic systems. As a conceptual application of the cylindrical converter, Fig. 27 depicts a five-converter heat pipe array with an estimated electrical output of 100 watts at 2.0 volts. Ten such heat pipe arrays emerging from a common heat source could yield an unconditioned power of 1 kilowatt.

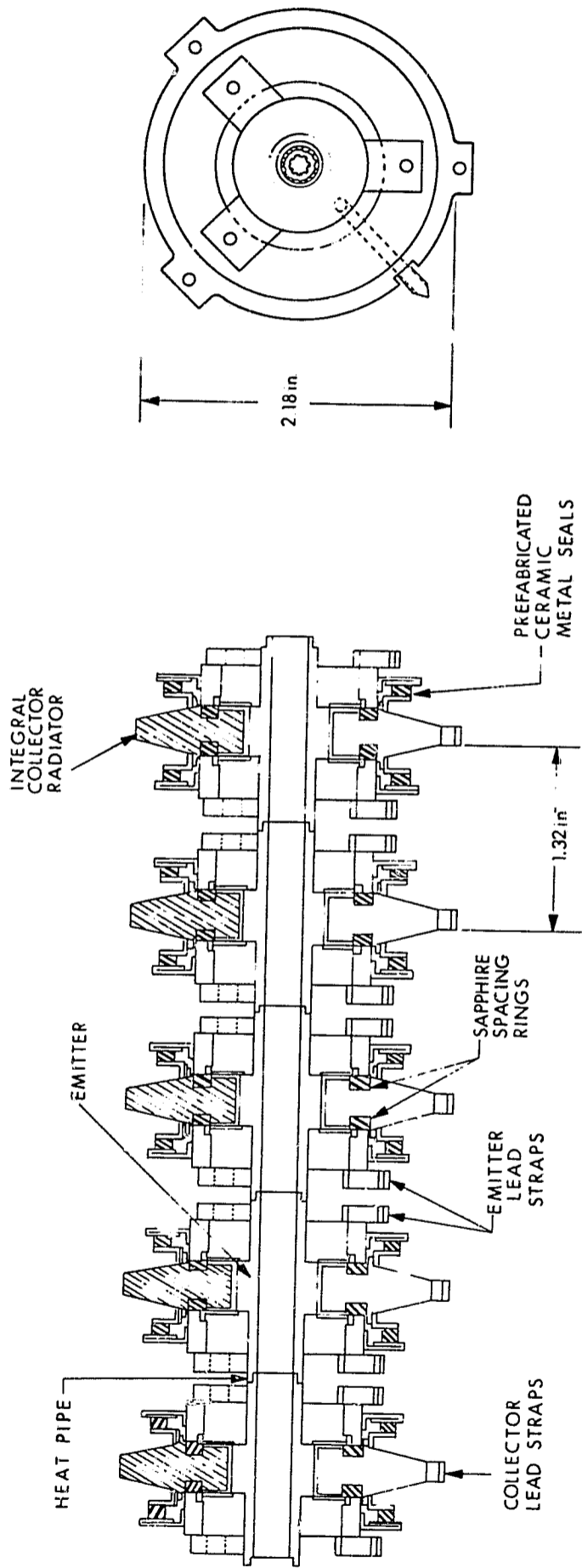


Figure 27. Potential Application of EOS Cylindrical Converter (Multiconverter Array)

The key features of the five-converter array are: (1) a heat-piped system produced by electron-beam-welding segmented heat-pipe cylindrical-converter sections, (2) cast sapphire tri-layers to electrically insulate the converter from the heat pipe, and (3) a completely pretested component system after the fashion of the set generator. This concept allows for the selection of series and parallel hookups to be made externally. Moreover, each converter contains a separate reservoir which will allow for individual converter testing and optimization.

Two of the cylindrical converters, SN109CA and SN109CB, have been fabricated and performance-tested. The SN109CA and SN109CB converter performance shows very close correlation and comparison to the SN109 planar converter. The results and comparisons are given in a following section.

4.1 FABRICATION AND ASSEMBLY PROCEDURE OF THE CYLINDRICAL CONVERTERS

One problem area peculiar to cylindrical converter geometries is that of maintaining the concentricity of the electrodes. Therefore, FOS has incorporated alignment pins into the design to establish and retain a 10% concentricity of the electrodes during fabrication. Also, electron-beam welding is used to join the subassemblies of the converter into the final diode configuration. Electron-beam welding has proved to be an effective means of joining the converter parts, in particular the emitter-to-emitter support structure. The instantaneous application of heat prevents excess warping, and the weld zone is small and ductile, which permits thermal cycling.

The principal subassemblies of SN109CA and SN109CB are shown in Fig. 28. They are the emitter, two emitter support structures, two ceramic spacers, two metal-to-ceramic seals, the collector-radiator, and the reservoir. Also shown are three alignment pins which are used in the fabrication procedure.

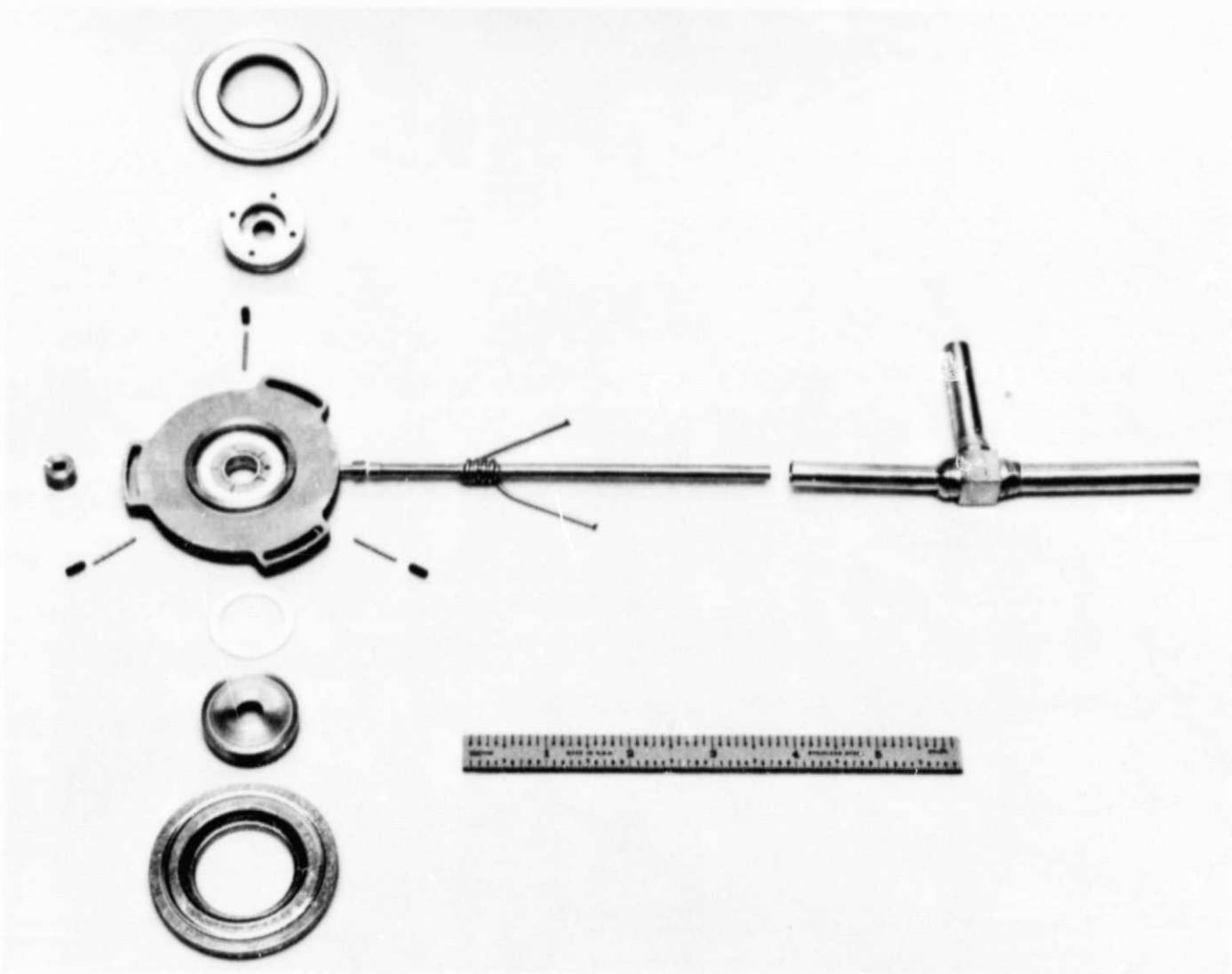


Figure 28. Cylindrical Converter Subassemblies

968154

Before the final assembly, the radiator portion of the collector-radiator is plasma-sprayed with a coating of Rokide "C" ($\epsilon = 0.78$) to provide a radiating area of $\approx 42 \text{ cm}^2$ of high emissivity for the rejection of heat.

The first step of assembly is to align the emitter concentrically in the collector-radiator. This is done by the use of a precision-machined sleeve, which is placed between the emitter and the collector. The alignment pins are then placed and set to retain the emitter concentric to the collector during the remaining assembly operations.

To complete the diode assembly, the following welds are made: two seal-subassembly to emitter-support structures, two seal-assembly to collector-radiator subassemblies, two emitter-to-emitter support structures, and three alignment pin closures.

The electron-beam welding of the prefabricated seal assembly to the collector-radiator niobium weld ring and the niobium emitter lead straps is done using a weld schedule of 150 kV at a current of 2.6 to 2.7 mA with a part rotation of 22 to 25 rpm. Also, electron-beam welds are made to join the emitter-to-emitter support structure (envelope), using a weld schedule of 120 kV at 2.0 mA. Attaching the emitter last has one main advantage in that it allows the emitter support structure to be stress-free when the emitter weld is made. The concentricity of the emitter to the collector is maintained during all electron-beam welding processes by the alignment pins. After the flange and emitter welds are made, the alignment pins are removed and the alignment pin channels are closed by electron-beam welding molybdenum plugs in the collector-radiator assembly on a schedule of 110 kV at 5.2 mA, with a part rotation of 40 rpm. This is done after the parts are preheated to approximately 1000°K . The exhaust tube assembly is joined to the

cylindrical converter assembly using an electron-beam welding schedule of 110 kV at 2.0 mA with rotation at 40 rpm. All electron beam schedules were predetermined by parameters established in feasibility experiments previously conducted on this program. They are outlined in Subsection 4.4 of Report 4006-Q-2.

After the diode assembly is completely welded, it is thermal-cycled to anticipated operating temperatures before final processing and high-purity cesium distillation.

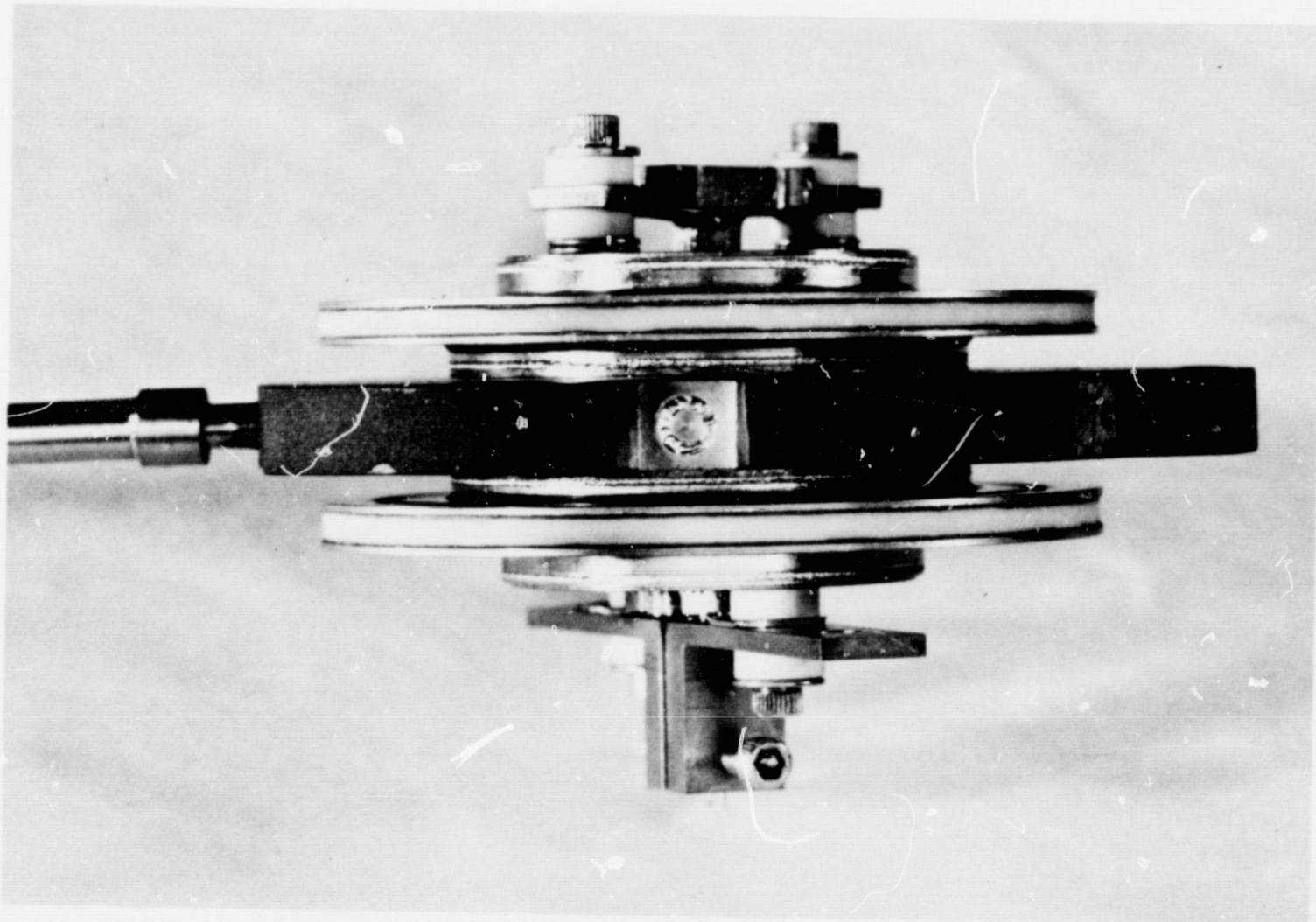
The completed diode exhaust assembly of SN109CA is shown in Fig. 29.

4.2 INSTRUMENTATION AND CYLINDRICAL CONVERTER TEST PROCEDURES

EOS uses two methods of testing thermionic converters which yield equivalent results. The first technique involves the steady-state dc measurement of converter current and voltage from a simply instrumented circuit, as shown in Fig. 30. The usual passive resistor is replaced with an electronic load that is capable of operating at constant voltage or constant current output from the converter. The emitter temperature is held constant at the testing temperature while the cesium reservoir and collector temperatures are adjusted for maximum converter output at various specified voltage levels.

Voltage output is measured across the converter terminals with a calibrated 0.5% or better voltmeter. Current output is measured as a millivolt drop across a calibrated 0.1% accurate shunt.

A second method used to obtain current-voltage data is to sweep the converter load line by impressing a 60 Hz voltage source upon a fixed converter operating point. An oscilloscope is used to monitor the sweep characteristics. The main advantage of this technique is that an entire I-V characteristic may be photographed with all element temperatures remaining constant.



106843

Figure 29. Completed SN109CA Diode Assembly

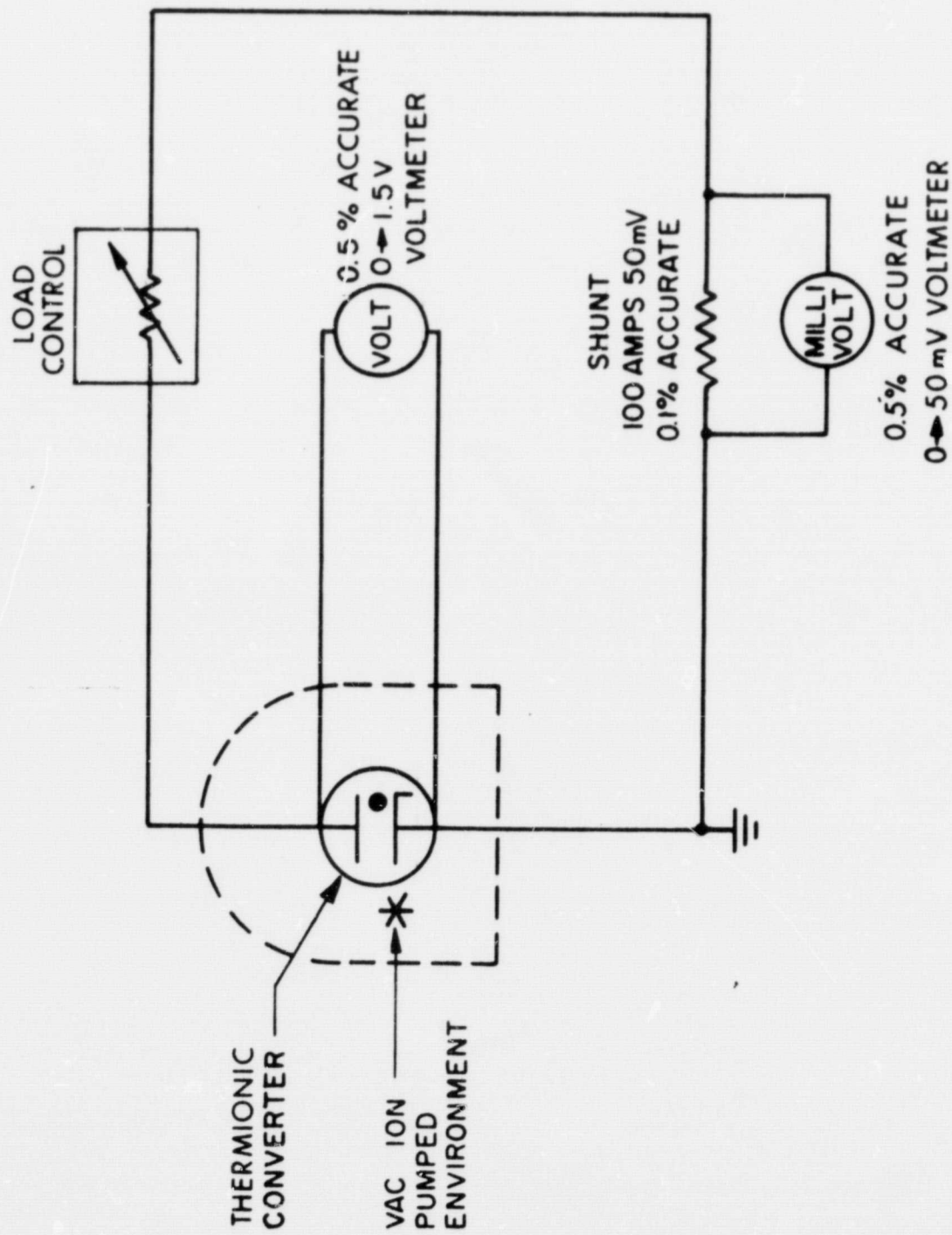


Figure 30. Electrical Circuit for DC Performance Testing of Thermionic Cylindrical Converters

Two types of temperature measuring instruments are used in the converter testing: micro-optical pyrometers and thermocouples. The cylindrical converter emitter temperature is measured by sighting the micro-optical pyrometer on an 8:1 to 10:1 depth-to-diameter hohlraum drilled parallel to the emitter surface. Temperature corrections due to transmission losses when sighting through a vacuum bell jar are calibrated from 1400° to 2200°K.

Thermocouple measurements of the cylindrical converters are made during testing at the cesium reservoir (2 couples), the collector (2 couples), the radiator (1 couple), and the seals (1 couple). All thermocouples have material continuity from the temperature measuring junction through the vacuum system and into the ice junction to prevent erroneous emf generation. All thermocouples are made from the same heat number as supplied by the vendor. The variation in millivolt response from these couples is approximately $\pm 0.5\%$ of the true temperature indicated by a secondary standard of platinum/platinum-10% rhodium.

The two cesium reservoir thermocouples are spot-welded to the reservoir tube assembly as close to the cesium liquid-vapor interface as can be determined. The immersion collector thermocouples are placed approximately 0.070 to 0.090 inch from the collecting surface. One thermocouple is spot-welded on the radiating portion of the collector-radiator assembly. It is placed so that the average radiator temperature can be monitored. The seal temperature is monitored by a thermocouple spot-welded to the emitter flange side of the ceramic-metal seal.

All thermocouple responses are measured on a Leeds and Northrop No. 8690 potentiometer that is 0.1% accurate or better.

4.3 PERFORMANCE TESTING OF SN109CA

Figure 31 is an optimized performance plot of the dc output of converter SN109CA under the following test conditions: (1) an emitter temperature of 1800°K true hohlraum temperature; (2) potential voltage leads placed at the converter terminals, not electrodes; and (3) all data points recorded under steady dc conditions.

Figure 32 shows the results of the current optimization for an emitter temperature of 1800°K and a constant output voltage of 0.4 volt. The power output density is 10.4 watts/cm^2 at 0.4 volt dc.* The tested efficiency of SN109CA operating at 10.4 W/cm^2 (0.4 volt x 49.0 amps) was 6.8%. However, the electron bombardment gun was not shielded and is quite inefficient as a heating source.

Figure 33 is a dc steady-state performance plot of SN109CA taken at an emitter temperature of 1700°K . The power output density is 6.1 W/cm^2 at 0.3 volt dc. The tested converter efficiency of SN109CA at 1700°K is 5.1%.

Figure 34 shows the current optimization for an emitter temperature of 1700°K at a voltage output of 0.3 volt.

4.4 PERFORMANCE TESTING OF SN109CB

SN109CB was tested using the same instruments, test setup, and test conditions as SN109CA (i.e., emitter temperature of 1800° and 1700°K (true hohlraum), potential voltage leads placed at the converter terminals, and all data points recorded under steady dc conditions).

* Based on a collector area of 1.88 cm^2 .

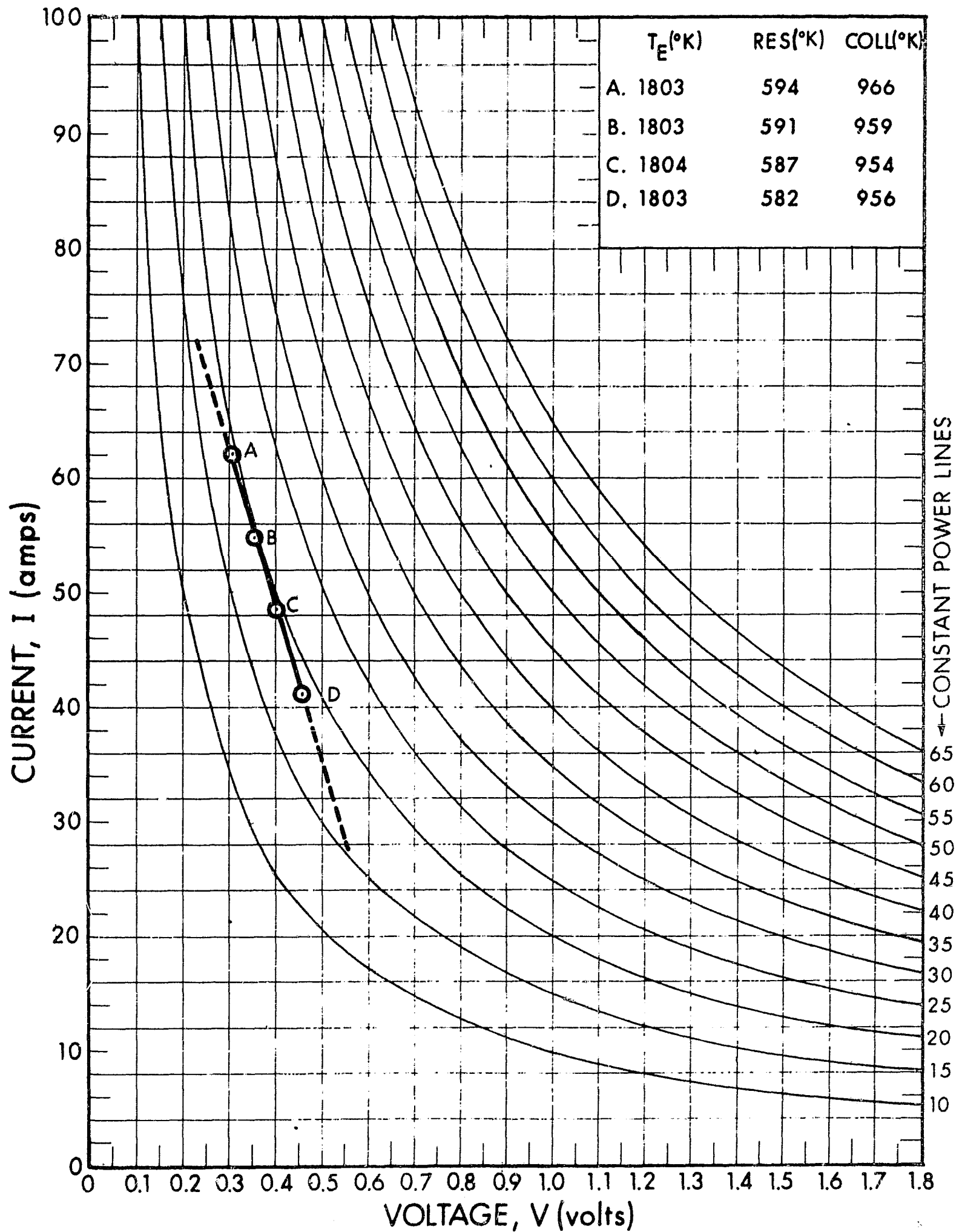


Figure 31. Performance Plot of SN109CA Cylindrical Converter Taken at the Design Emitter Temperature of 1800°K (true hohlraum)

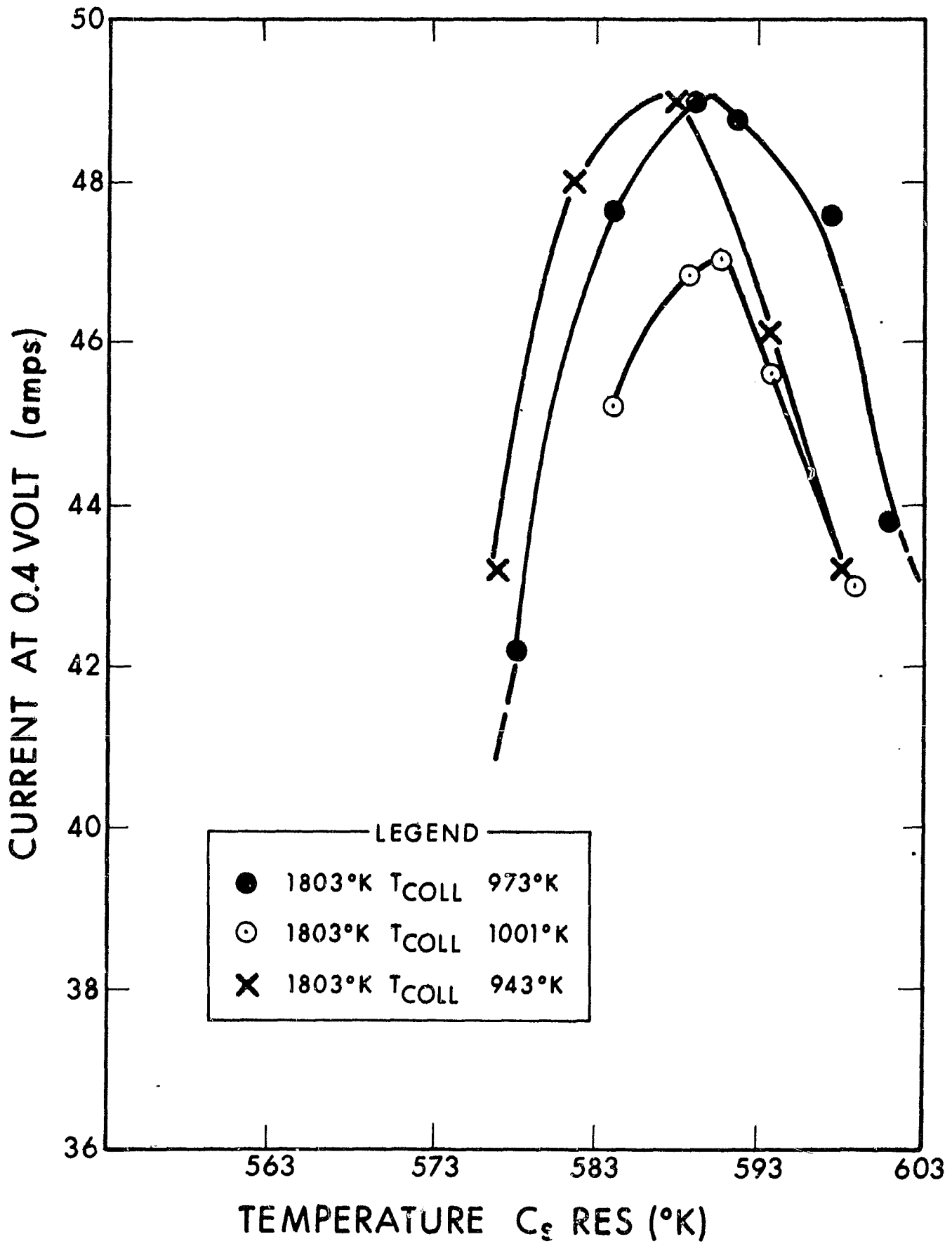


Figure 32. Current Optimization Plot of SN109CA Taken at the Design Operating Emitter Temperature of 1800°K (true hohlraum)

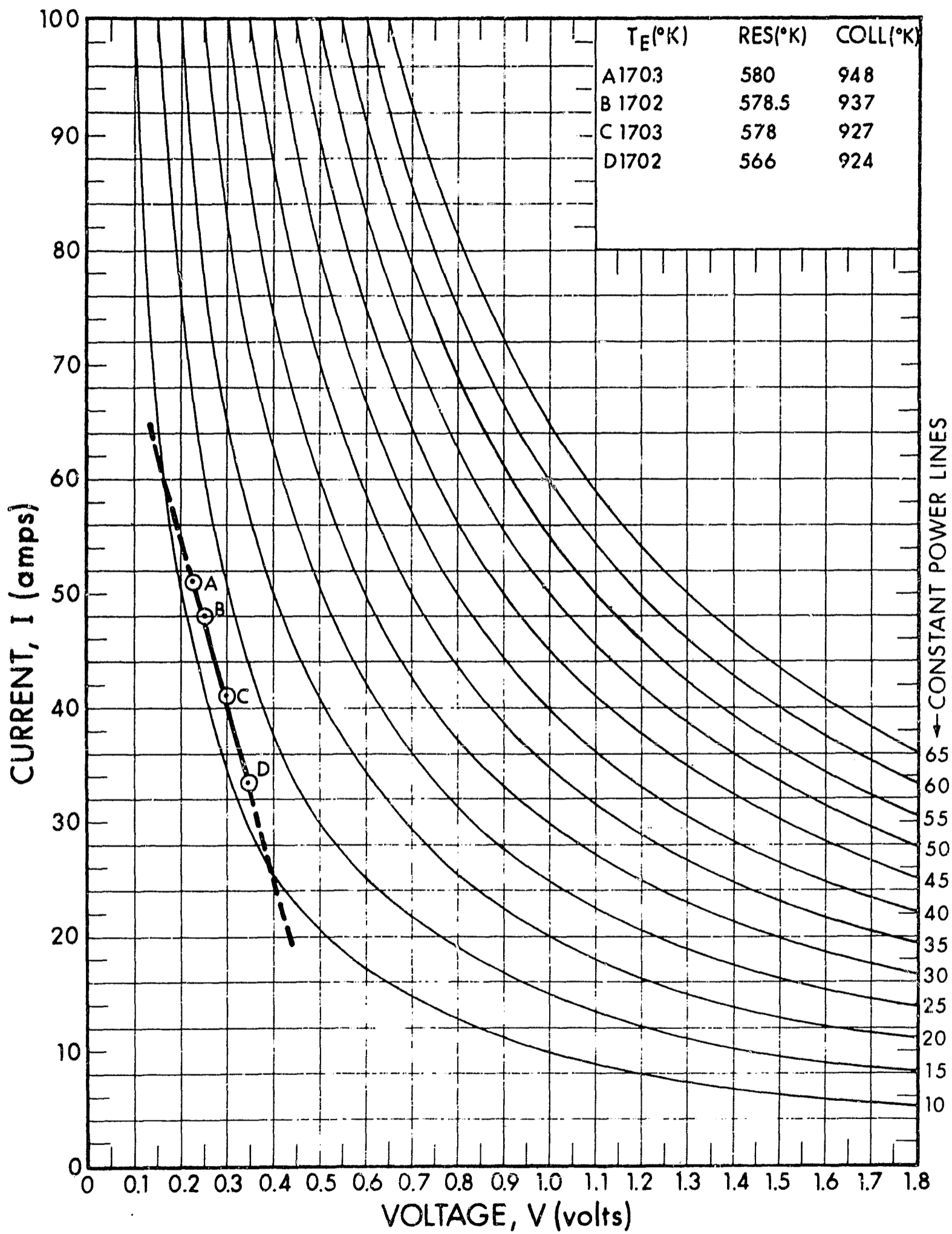


Figure 33. Performance Plot of SN109CA Cylindrical Converter Taken at an Emitter Temperature of $1700^{\circ}K$ (true hohlraum)

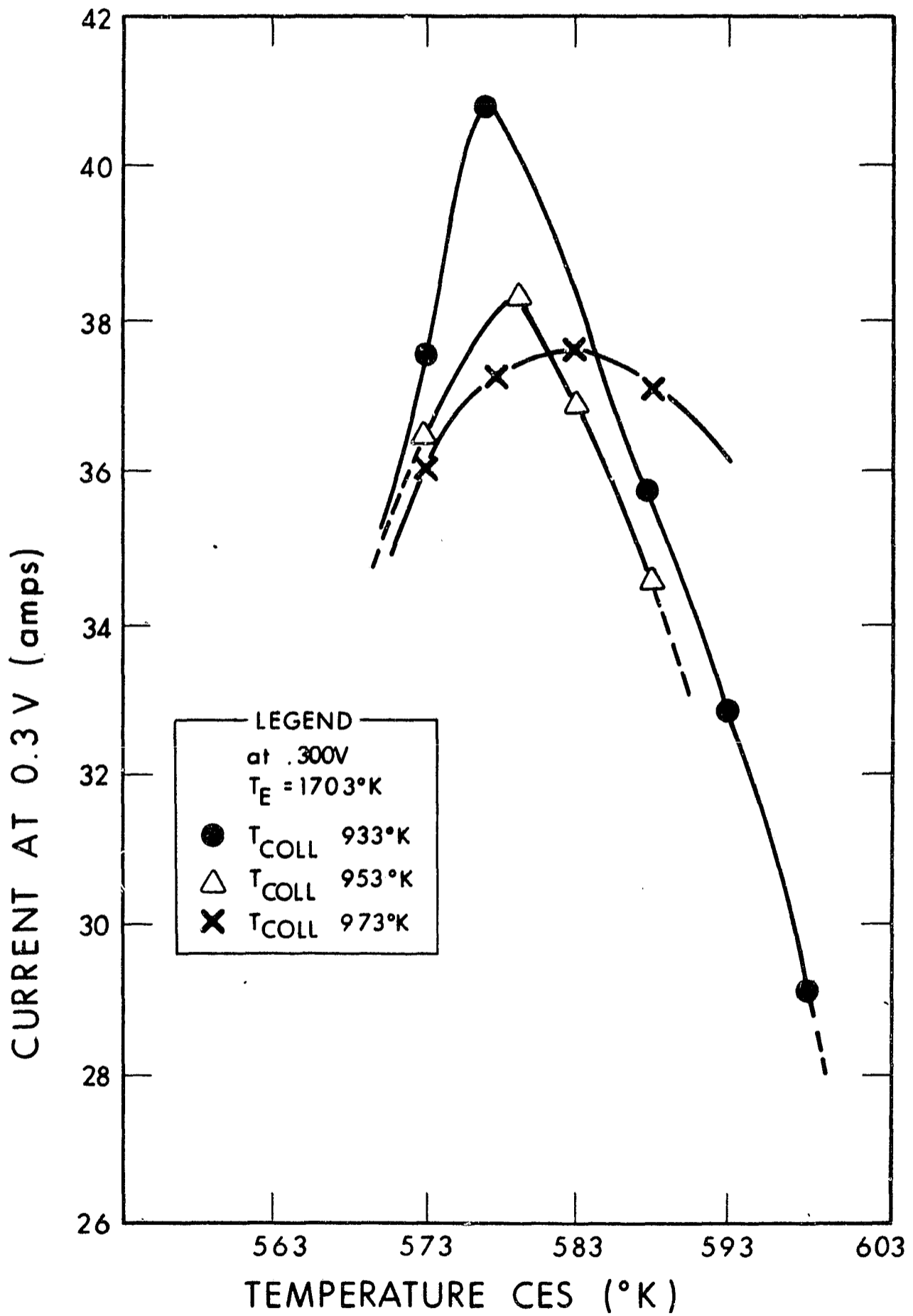


Figure 34. Current Optimization Plot of SN109CA Taken at an Emitter Temperature of 1700°K (true hohlraum)

Figure 35 is an optimized performance plot of the dc output of converter SN109CB. The output power density at 0.4 volt dc is 10.2 watts/cm².^{*} The tested efficiency using an unshielded electron bombardment gun was 6.4%.

Figure 36 shows the results of the current optimization for an emitter temperature of 1800°K at a constant output voltage of 0.4 volt.

Figure 37 is a steady-state dc performance plot of SN109CB taken at an emitter temperature of 1700°K. The power output density is 6.4 watts/cm² at 0.3 volt.^{*} The tested converter efficiency at 1700°K is 4.9%.

Figure 38 shows the current optimization for an emitter at 1700°K, taken at a constant voltage output of 0.3 volt.

4.5 CORRELATION AND COMPARISON OF CYLINDRICAL CONVERTERS SN109CA AND SN109CB TO PLANAR CONVERTER SN109

SN109CA and SN109CB were built in an attempt to demonstrate a one-to-one correspondence with the performance of a SN109-type planar converter. To reproduce the performance of SN109 at its design point of 1800°K, SN109CA and SN109CB were built with the same electrode materials, electrode areas, and interelectrode spacing.

The results of the performance and current optimization plots (Figs. 31 through 38) of SN109CA and SN109CB are within 1 amp of one another, which can be interpreted as a difference of approximately 2%. Close agreement is also seen with the output obtained from the vapor-deposited rhenium variable parameter test vehicle at 1800° and 1700°K.

^{*} Based upon a collector area of 1.88 cm².

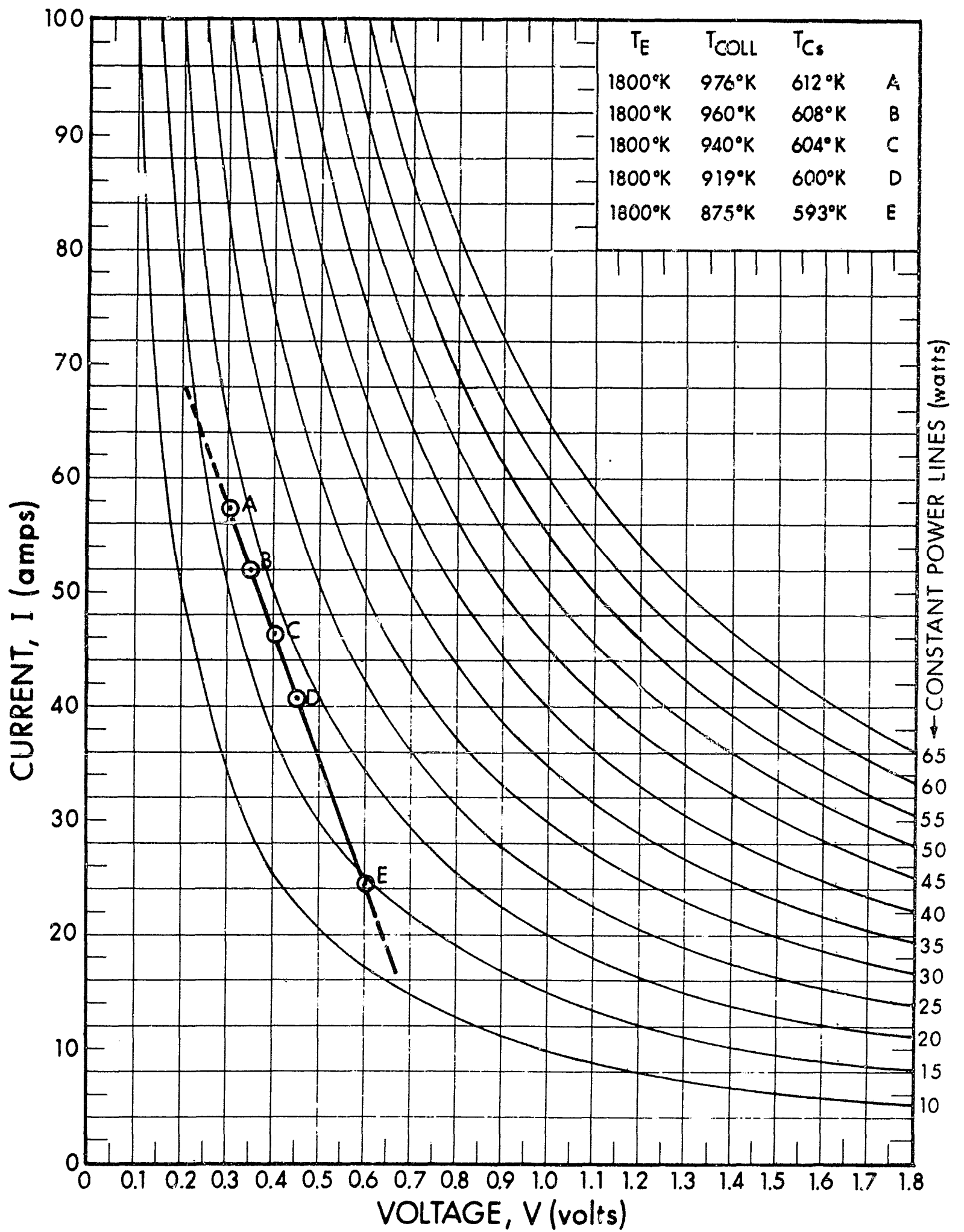


Figure 35. Performance Plots of SN109CB Taken at the Design Emitter Temperature of 1800°K (true hohlraum)

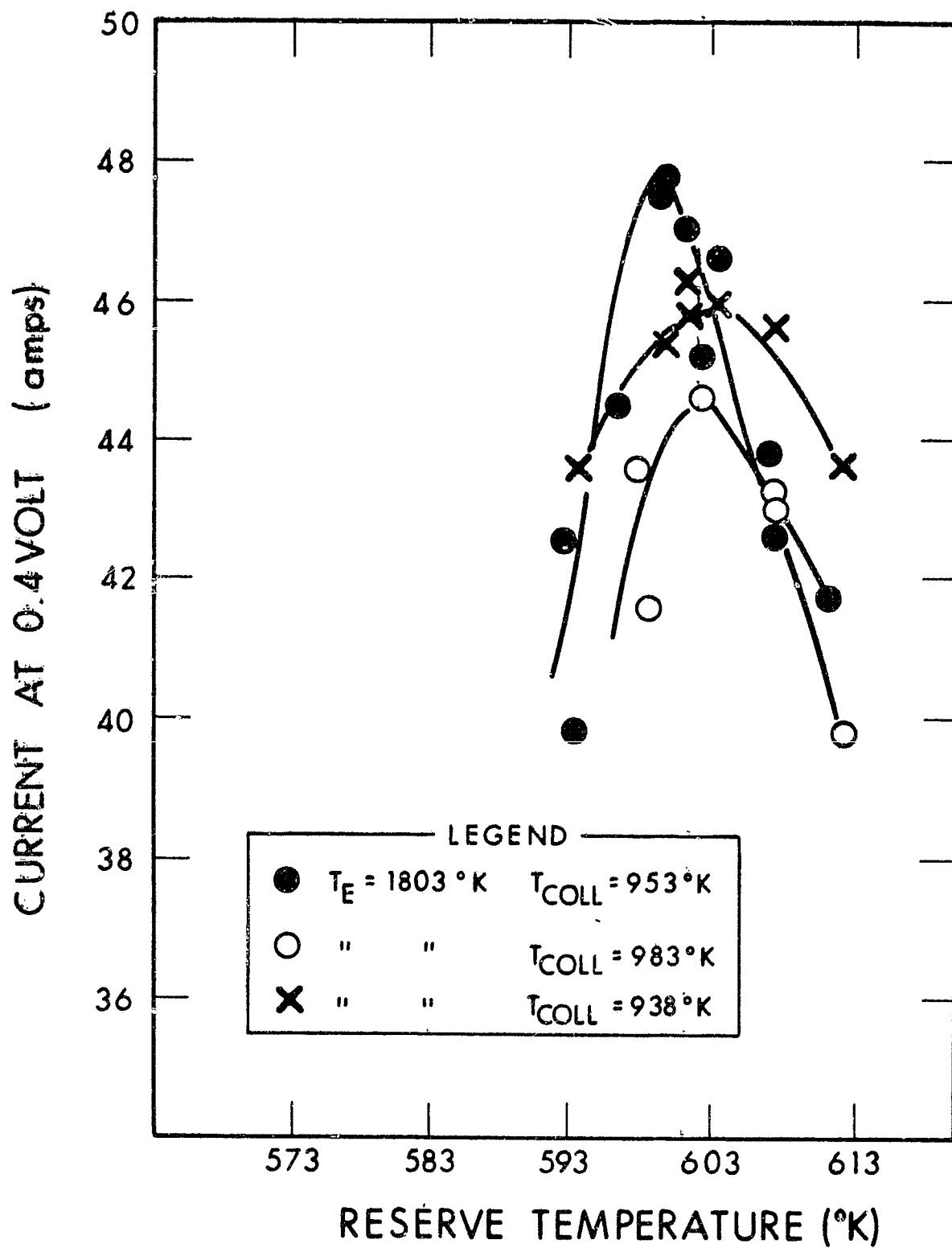


Figure 36. Current Optimization Plot of SN109CB Taken at the Design Operating Emitter Temperature of 1800°K (true hohlraum) and a Constant Voltage Output of 0.4 Volt

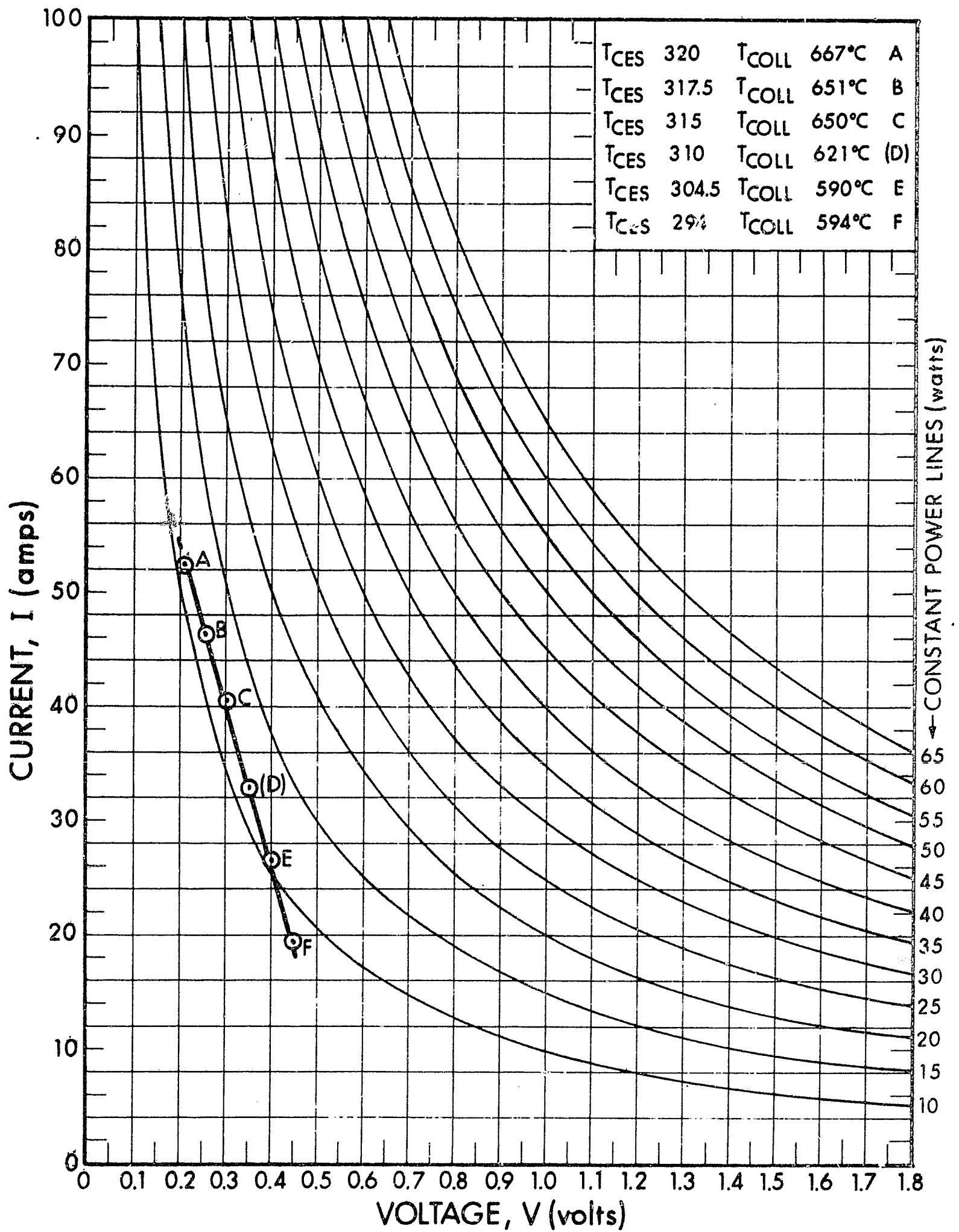


Figure 37. Performance Plot of SN109CB Taken at 1700°K (true hohlraum)

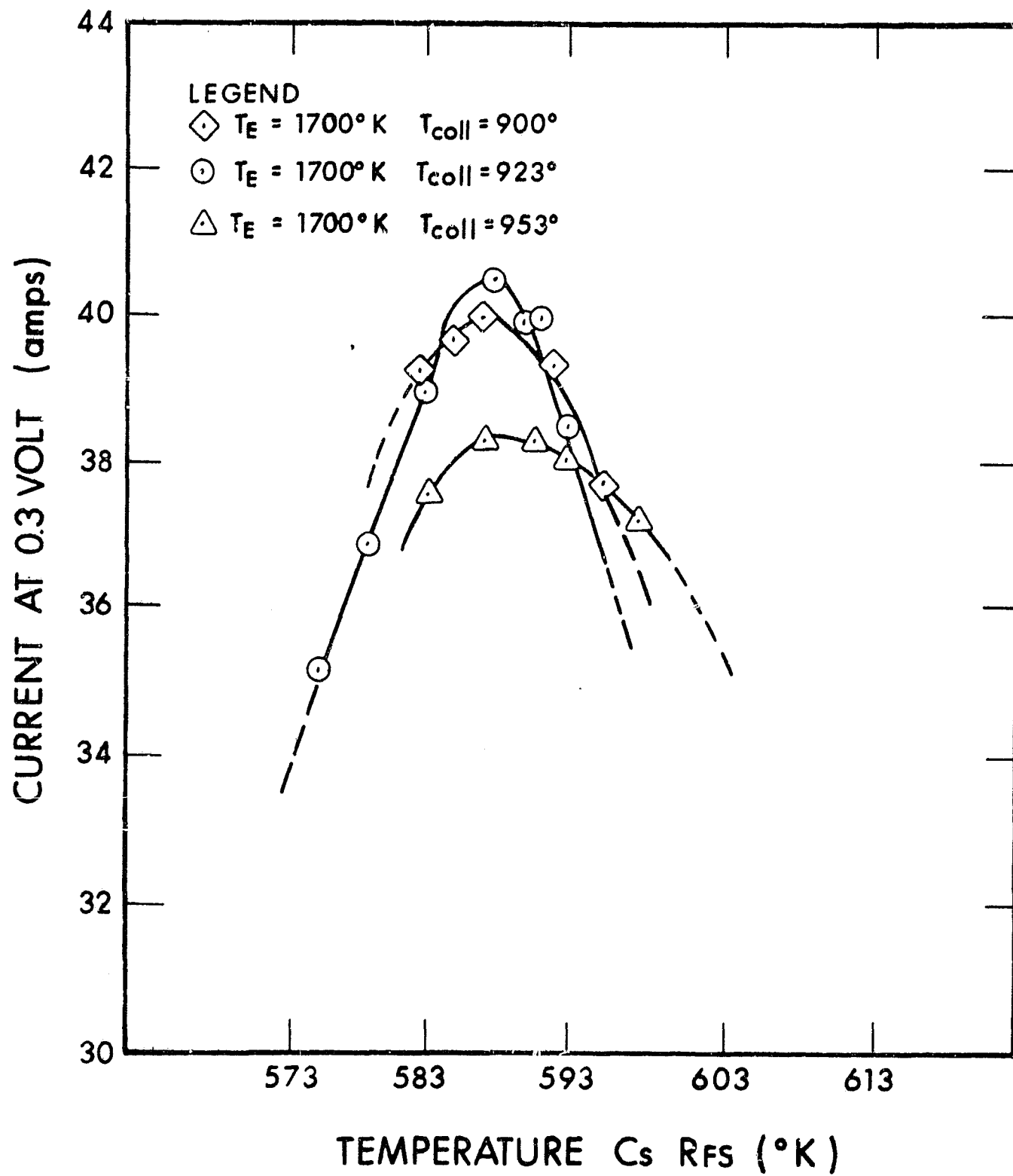


Figure 38. Current Optimization Plot of SN109CB Taken at an Emitter Temperature of 1700°K (true hohlraum) and a Constant Voltage Output of 0.3 Volt

Table IX shows the comparison of planar converter SN109 to the cylindrical converters SN109CA and SN109CB at 1800°K.

TABLE IX

COMPARISON OF PLANAR CONVERTER SN109 TO CYLINDRICAL CONVERTERS
SN109CA and SN109CB AT 1800°K

	<u>Planar SN109</u>	<u>Cylindrical SN109CA</u>	<u>Cylindrical SN109CB</u>
Emitter temperature (true hohlraum)	1800°K	1800°K	1800°K
Power output (V x A)	0.40 x 49	0.40 x 49	0.40 x 48
Power density (W/cm ²)	10.4	10.4	10.1
Emitter area (cm ²)	2.0	2.0	2.0
Collecting area (cm ²)	1.88	1.88	1.88
Electrode material	Vapor- deposited rhenium	Vapor- deposited rhenium	Vapor- deposited rhenium

REFERENCES

1. Wichner, R., and Pigford, T. H., Thermionic Conversion Specialist Conference, Houston (1966)
2. Campbell, A. E., High-Performance Thermionic Converters, Contract 951225, September 2, 1966.
3. Campbell, A. E., and Jacobson, D. L., Thermionic Research and Development Program, Contract NAS7-514, March 1, 1968
4. Cleveland Refractory Metals, Technical Properties Data, Rhenium and Rhenium Alloys
5. EOS 4006-Q-1, pp 40-41.